NASA CR- 164,853

NASA-CR-164853
19810025425

Final Report

Grant No. NASA NSG 1567

INVESTIGATION OF DIRECT INTEGRATED OPTICS MODULATORS

Submitted to:

National Aeronautics and Space Administration
Langley Research Center
Hampton, Virginia 23665

Submitted by:

T. E. Batchman
Associate Professor

G. M. McWright
Graduate Student Participant

Report No. UVA/528171/EE81/101

September 1981

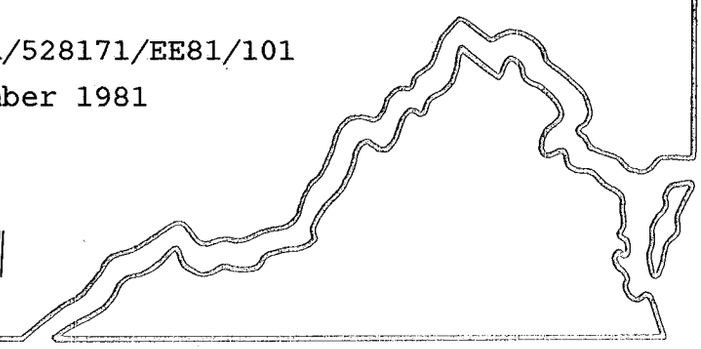

SEMICONDUCTOR DEVICE LABORATORY
DEPARTMENT OF ELECTRICAL ENGINEERING
SCHOOL OF ENGINEERING AND APPLIED SCIENCES
UNIVERSITY OF VIRGINIA

SDL

Final Report

Grant No. NASA NSG 1567

Investigation of Direct Integrated Optics Modulators

Submitted to:

National Aeronautics and Space Administration
Langley Research Center
Hampton, Virginia 23665

Submitted by:

T. E. Batchman
Associate Professor

Graduate Student Participant
G. M. McWright

Report No. UVA/528171EE81/101

September 1981

Abstract

The purpose of this program was to study direct optical modulation techniques applicable to integrated optical data preprocessors. After reviewing several techniques potentially useful in direct modulators, it was decided to concentrate our research effort on the analysis and fabrication of a field effect type modulator. A series of computer modeling studies were performed to determine the effects of semiconductor claddings on the fields of propagating waves in planar dielectric waveguides. These studies predicted that changes in the propagation characterisitics of waveguides clad with silicon and gallium arsenide could be made large enough to be useful in modulators. These effects are dependent on the complex permittivity and thickness of the cladding. Since the conductivity of the cladding can be changed by the photon generation of hole-electron pairs, incoherent light may be used as the input to modulate a coherent light beam. Waveguides were fabricated and silicon claddings were applied to verify the theoretical predictions.

Table of Contents

I. INTRODUCTION

An integrated optics holographic comparator has been proposed (1) for use as a data preprocessor for airborne optical sensors. This device, as presently proposed, requires the conversion of the sensor optical signal into an electrical signal which then modulates a coherent optical beam by means of a set of metal electrodes deposited on a lithium niobate waveguide (Figure 1). This technique introduces noise and extra hardware because of the needed signal conversion from optical to electrical.

The objective of this investigation was to determine the feasibility of direct modulation of a coherent optical beam by an incoherent optical source to eliminate some of the above problems. Several direct modulation techniques were investigated during the first year of this study. One technique investigated was the metal-barrier-metal, or more commonly metal-oxide-metal device (MOM), which makes use of tunneling effects through a barrier region. While the MOM device shows great promise for this application, it is still in the early stages of research and its ability as an optical modulator in an integrated optical circuit has yet to be investigated. Two other techniques currently being developed are the Pockels-Readout-Optical Modulator (PROM) type memory and display devices and a spatial light modulator being developed by M.I.T. These devices were discussed in Section 2 of the first annual report (2).

The concept selected for investigation during the latter part of this study was that of a photon induced change in conductivity in a semiconductor clad optical waveguide (Figure 2). The background investigation and preliminary computer prediction on

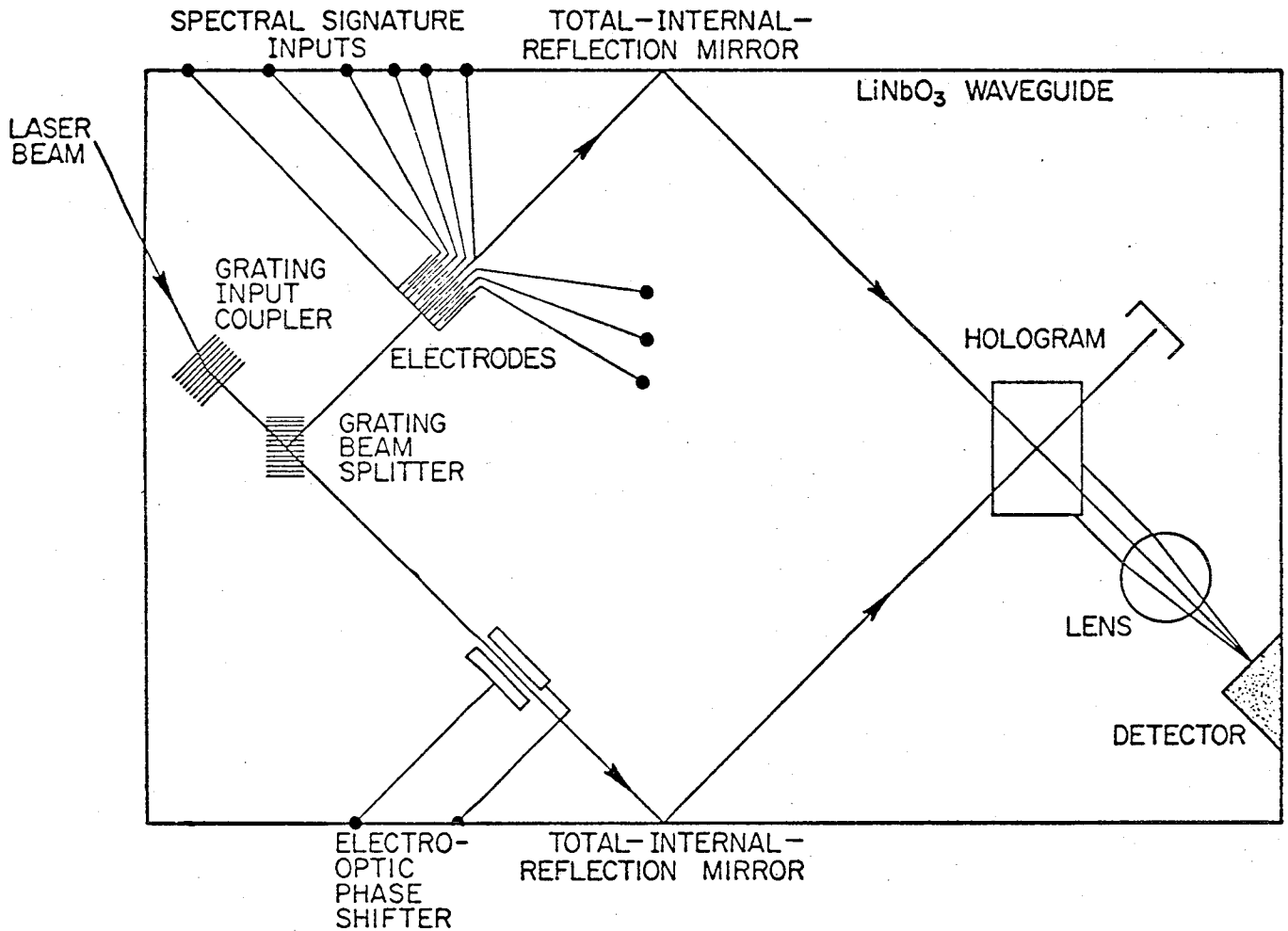

Figure 1. Schematic of One Configuration of the Integrated Optics Holographic Comparator. (Ref. 1)

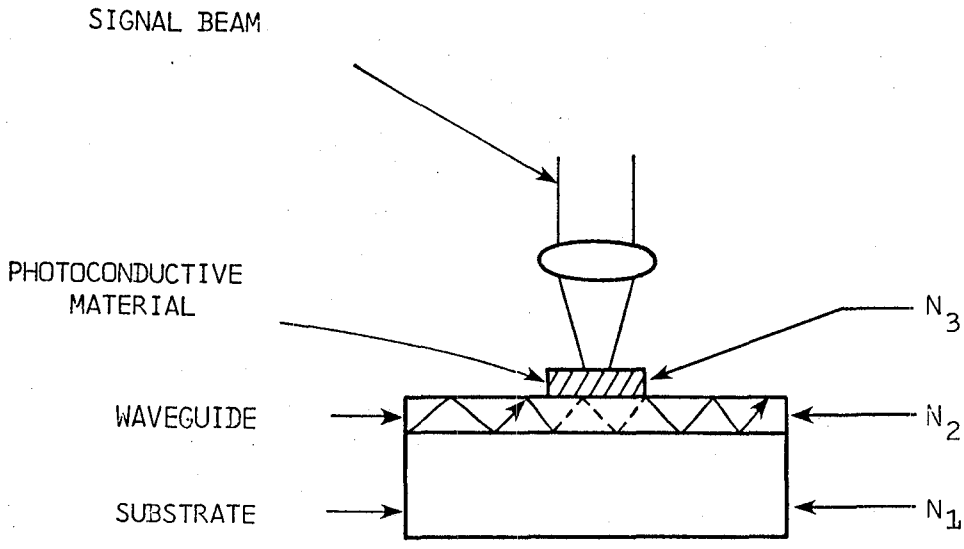

Figure 2. Photoconductive Modulator

the feasibility of using a clad waveguide type modulator are presented in detail in references 2 and 3. Section 2 of this report briefly summarizes the results of these previous studies along with attempts at experimental verification of the predicted photon modulation effect.

Section 3 of this report discusses the results of computer predictions on the effects of changing the real part of the complex permittivity of the semiconductor cladding. It was orginally postulated that deposited silicon films being used in the experiments might have a significantly different permittivity than that used for the computer predictions. The predicted results did not verify this postulate and thus additional experimental studies have been initiated as discussed in Section 7.

In order to better understand the results of the computer predictions and to develop a theory for the predicted modulation effects, the fields in the waveguide, substrate and cladding region were calculated and plotted. Section 4 presents the results of these calculations and the multilayer interference theory used to explain the computer predictions.

Unfortunately the modulation scheme being studied suffered from an extremely high attenuation due to the semiconductor cladding behaving as lossy dielectric. In Section 5 the results of attempts to reduce this attenuation through the addition of a buffer layer between the waveguide and the cladding are presented. The computer predictions indicate a significant reduction is possible through the use of a proper buffer layer.

Because of a number of problems which were experienced in depositing good photoconductive silicon films, selemium-clad waveguides were investigated. It is shown in Section 6 that selemium willproduce the same photon modulation effects as predicted for silicon and can thus be used if a suitable deposition systems is found.

Section 7 discusses experimental results of numerous studies on the temperature degradation occuring in ion exchanged waveguides and the design of new experimental measurement devices. The effects of exposing ion-exchanged waveguides to elevated temperatures for short periods of time were investigated to determine what methods of depositing semiconductor films on the waveguides were feasible or whether sputtered waveguides would be required. The design of a new series of experimental devices to be used in future measurements is also discussed in this section.

II. SEMICONDUCTOR-CLAD DIELECTRIC WAVEGUIDES: SUMMARY OF PREVIOUS RESEARCH

In this research, a planar waveguide configuration has been used for all computer modeling and fabrication. A semi-infinite glass substrate (refractive index N_1) covered first with a waveguide material of refractive index N_2 such that $N_2 > N_1$ and then a layer of semiconducting material forms the waveguide structure (Figure 2). The order of the dielectric and semiconductor layers is reversible. The fourth layer is air in all cases and for all calculations the waveguide material was polystyrene although any dielectric with a similar refractive index will produce the same results.

This basic structure has been analyzed utilizing classical electromagnetic theory and has been found to support propagation in the waveguiding region with a set of fields charcterized by:

$$\overline{E} = \overline{E}_{xyz}\, e^{j\omega t-\gamma z}$$

$$\overline{H} = \overline{H}_{xyz}\, e^{j\omega t-\gamma z} \qquad (2.1)$$

where γ = $\alpha + j\beta$, propagation constant

ω = radian frequency of propagation wave

α = attenuation constant (nepers/meter)

β = phase constant (radian/meter)

Each propagating path is characterized by its own propagation constants α_i and β_i. In order to understand a

structure's physical behavior, we must solve for α and β. The relationship we must solve is the dispersion relationship, which relates α and β to the physical properties of the structure and to the characteristics of the exciting wave (i.e. frequency). For the previously described structure, such a relationship has been derived (4). The general technique and result for this structure is as follows (2):

(1) It is assumed that all materials except the semiconductor are approximately lossless and that propagation is in the z direction.

(2) The nonzero components of the TE and TM modes are determined and substituted into the wave equation.

(3) The wave function is obtained by solving the wave equation. By invoking the condition of continuity of the wave function and by forcing the field components to satisfy Maxwell's boundary conditions, the dispersion relation is obtained:

$$K_{x3}\, t_3 = \tan^{-1}\left[\frac{K_{31}\frac{P_{x1}}{K_{x3}} + K_{32}\frac{P_{x2}}{K_{x3}}\tanh P_{x2}\, t_2}{1 - K_{21}\frac{P_{x1}}{P_{x2}}\tanh P_{x2}\, t_2}\right] + \tan^{-1}\frac{K_{34}\, P_{x4}}{K_{x3}} + n\pi \qquad (2.2)$$

where $K_{ij} = 1$ for TE modes

$K_{ij} = \varepsilon_i/\varepsilon_j$ for TM modes

$P_{xi} = [(\beta^2 - \alpha^2 - \varepsilon_i' K_o^2) + j(\varepsilon_i'' K_o^2\, 2\alpha\beta)]^{1/2}$

$K_{xi} = [(\varepsilon_i K_o^2 - \beta^2 + \alpha^2) + j(2\alpha\beta - \varepsilon_i'' K_o^2)]^{1/2}$

$n = 0, 1, 2$ = mode order

$K_o = 2\pi/\lambda$

$\varepsilon_i = \varepsilon_i' - j\varepsilon_i''$ = complex permittivity of region i.

Because this is a transcendental equation, it has been solvable only by numerical techniques. Two separate approaches have been used to solve this, and both have given identical results. For the remainder of this work, primary attention will be focused on α and β for the guiding region (N_3).

One attempt to solve the relation involves a razor search technique used by Bandler and Macdonald (5). In this program, the operator selects initial guesses for α, β and convergence factors for error estimation. The computer then uses a random walk technique to calculate values for α and β satisfying the dispersion relation. Results are based on input of the above mentioned data plus the physical structure parameters set at the beginning of the run. This program (called WAVE) has one inherent weakness due to the requirement for finding the tangent function. While the tangent may be found by at least two different methods both produce questionable results as points of discontinuity are approached or when the tangent function changes quadrants. This was a problem of concern when t_2 became very small ($t_2 << 1$ μm).

A second method of solving for α and β is to formulate the problem as an eigenvalue problem as described by Smith and Mitchell (6). In this approach, characteristic matrices are created for each layer based on given material parameters. These matrices are then solved for the required eigenvalues and thus α and β. The solutions obtained with this program (called

MODEIG) are identical to those obtained with WAVE at all points plus it is able to compute points at the tangent discontinuities which WAVE cannot.

Before beginning work on this grant, changes in the attenuation of progagating modes in a semiconductor clad waveguide (Figure 2) had been observed as the semiconductor cladding material was varied (Figure 3). Any lossy material has a complex permittivity given by

$$\hat{\varepsilon} = \varepsilon' - j\varepsilon'' = \varepsilon' - j\,\frac{4\pi\sigma}{\omega}$$

where ε' is the real part of the permittivity and σ is the conductivity of the material at frequency ω. This can also be expressed in terms of the complex refractive index

$$\hat{n} = \varepsilon^{1/2} = n - j\,k$$

where k is the extinction coefficient.

It was noted that the real part of the complex permittivty is about the same for germanium (17.4) and gallium arsenide (14.3), but the conductivity at λ = 632.8 nm is quite different [Ge, $\sigma = 3.2 \times 10^2$ (ohm cm)$^{-1}$ and GaAs, σ = 25.4 (ohm cm)$^{-1}$]. Figure 3 shows the predicted variation in attenuation for these two materials when the cladding thickness is semi-infinite ($t_2 = \infty$ in Figure 2b). While this was not a large change in α, it indicated an important phenomenon to be investigated. The fact

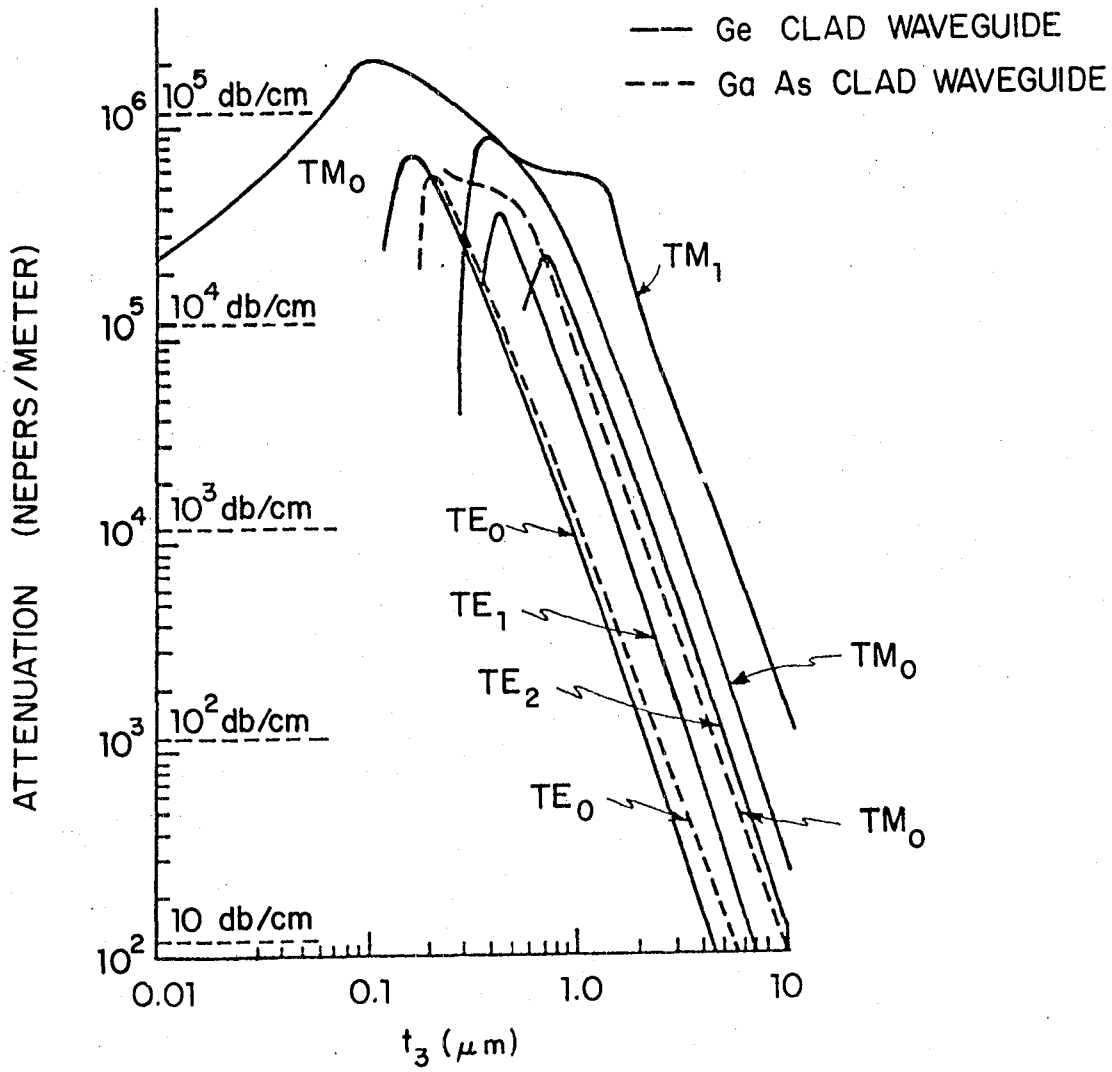

Figure 3. Attenuation of Ge and GaAs Clad Waveguides

that a change in the conductivity of the cladding material changesthe attenuation of the propagating made in the waveguide then leads one to predict modulation effects since the conductivity of a semiconductor can be changed through photon generation of hole-electron pairs. This has recently been demonstrated in microwave guides using semiconductor cladding (7).

Having noted the effect of a change in conductivity on the attenuation of a waveguide, the next step was to try to enhance the magnitude of the effect through proper choice of cladding materials, cladding thickness and waveguide thickness (t_3). Allowing t_3 to vary as the conductivity was changed only shifted the characteristic attenuation curves (as in Figure 3) up or down and produced no detectable change in the phase characterisitc of the waveguide.

Previous experience indicated that the attenuation normally decreased as the cladding thickness (t_2) was decreased so the next step was to vary the cladding thickness while also varying the conductivity to see if this had any beneficial results. The results obtained were perplexing since they were entirely different than anything previously observed. Figure 4 shows the results for the GaAs clad waveguide as t_2 is varied. Not only does the attenuation vary with conductivity but it also seems to oscillate after the cladding thickness decreases past 1.0 μm. This oscillation had never been observed before so it raised a number of questions about possible errors in the computer program. The most significant result of these predictions was that the conductivity ppeared to have a relatively large affect

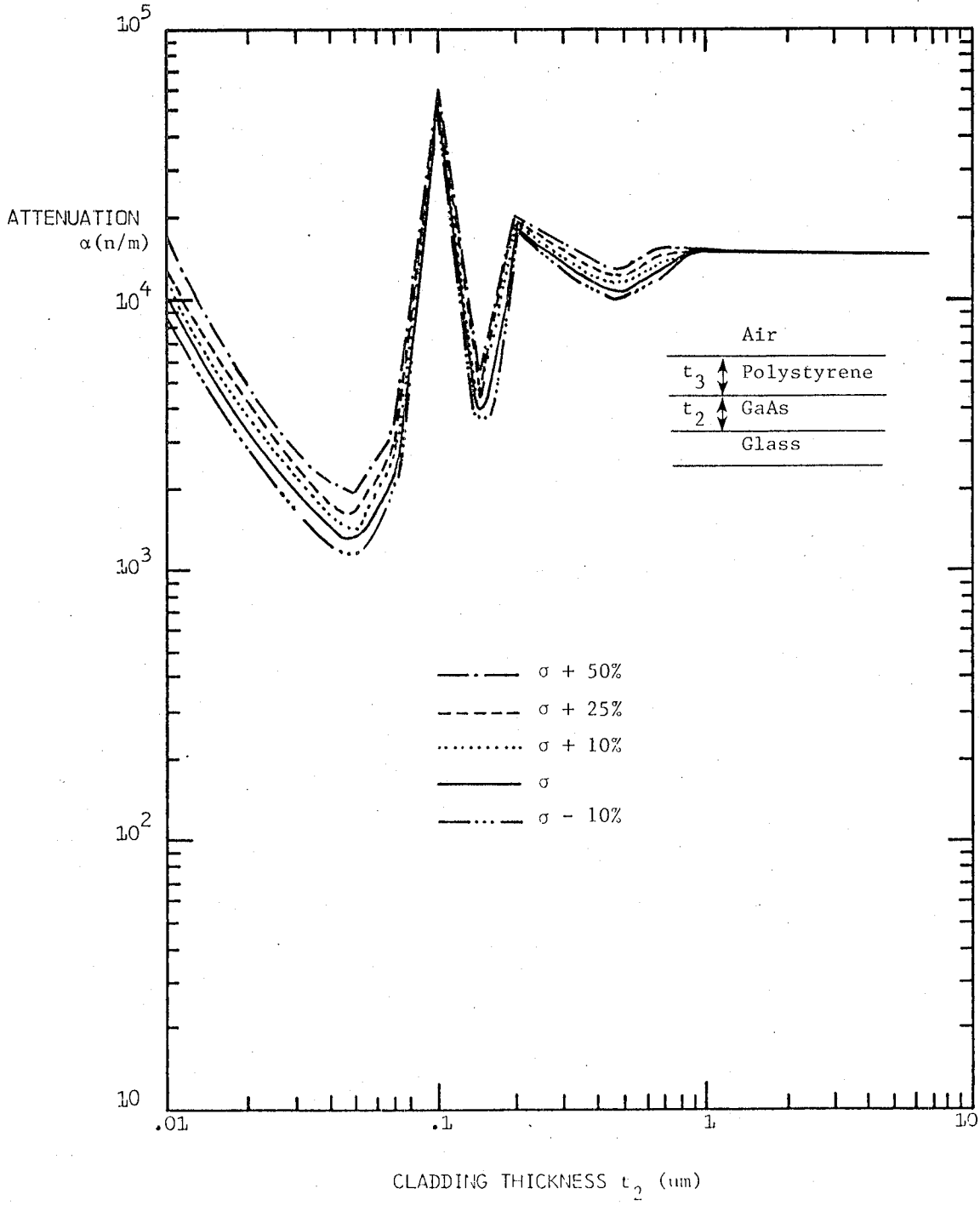

Figure 4. Variation of Attenuation with GaAs Cladding Thickness for the TE_o Mode (t_3 = 1.0 um)

on the attenuation at certain cladding thicknesses. Since only a few thicknesses were used in calculating Figure 4, additional points were calculated to detemine the oscillation frequency.

Figures 5 and 6 show the variation of attenuation with t_2 for a fixed conductivity (normal value) after the additional points were calculated. Now the oscillation is even more pronounced and there seems to be a discontinuity in the mode index curve at 0.09 μm. At thicknesses greater than 0.1 μm the mode index curve appears to be continuous. As noted before, this oscillatory behavior had never been observed before in any of our calculations but after verification using both computer programs the conductivity (σ) and cladding material were varied. The three most common semiconductors were selected to see what effect the material permittivity had on the results. Since GaAs had already been investigated, silicon and germanium were used as claddings. The complex permittivities and refractive indices are shown in Table I which follows.

Table I

Semiconductor Parameters at λ = 632.8 nm

Material	Permittivity		Refractive Index	
	ε'	ε''	n	k
GaAs	14.3	1.21	3.79	0.16
Silicon*	16.76	1.75	4.1	0.213
Germanium*	14.43	19.54	4.4	2.22

*values for amorphous thin films

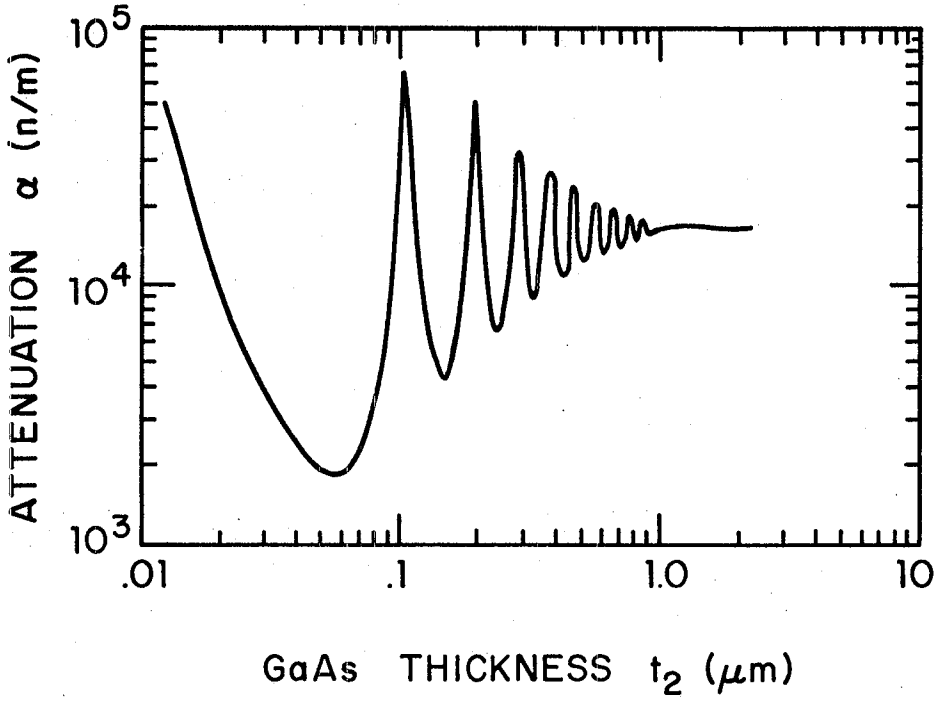

Figure 5. GaAs/Air-Clad Waveguide Attenuation vs. t_2 (TE_o mode, normal conductivity; t_3 = 0.8 μm)

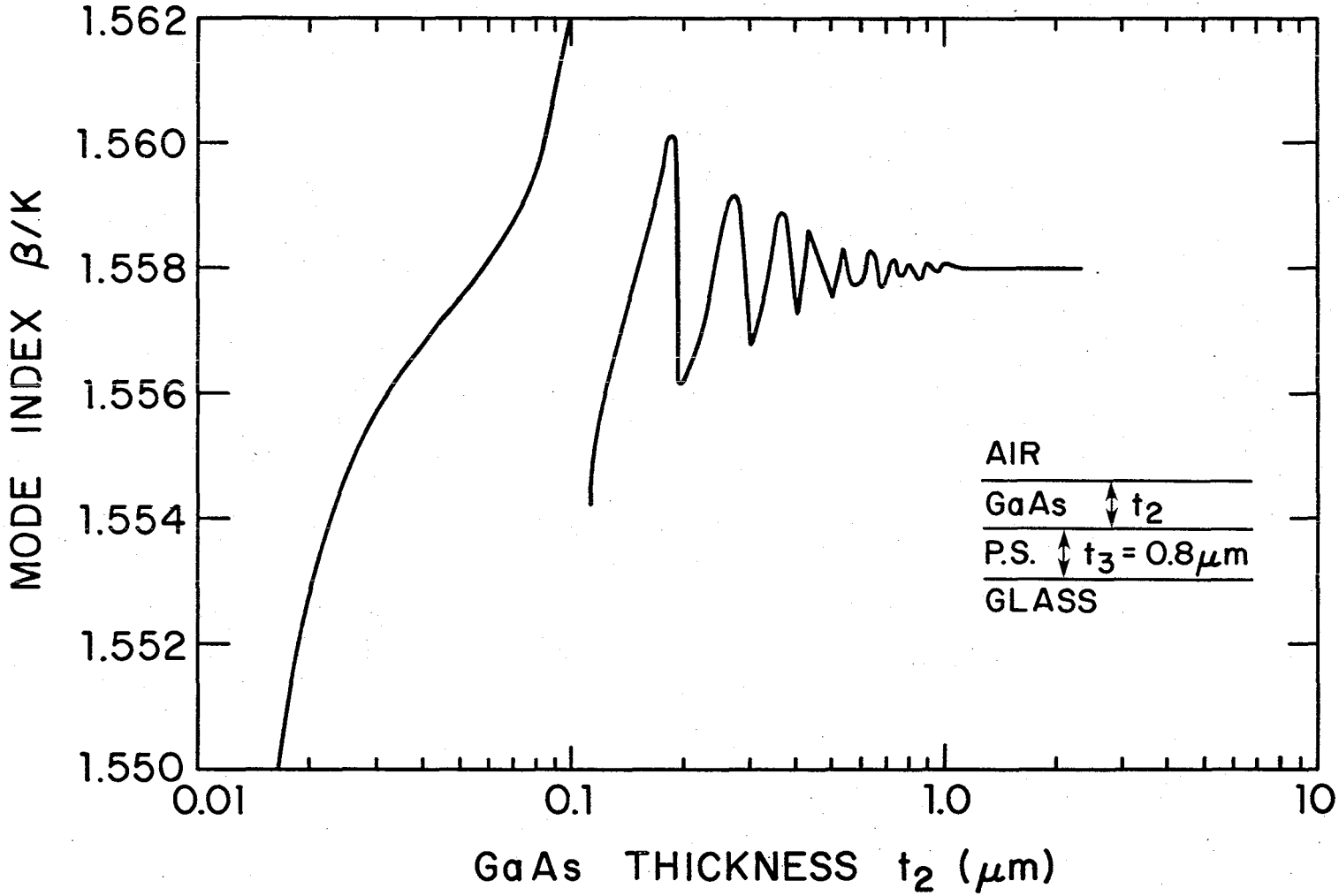

Figure 6. GaAs/Air Clad Waveguide

Note that the relative magnitudes of the real and imagninary parts of the complex permittivity of gallium arsenide and silicon are the same. Germanium, however, has a considerably higher imaginary part (conductivity) than either silicon or gallium arsenide. If material conductivity has any effect on the characteristics observed it should be evident in germanium. Figures 7, 8, 9, and 10 show the results for silicon and germanium. As might be expected, silicon exhibits characteristics nearly identical to those of GaAs. Germanium shows almost none of the oscillations which were characterisitcs of GaAs which can be attributed to the large conductivity used for germanium in this calculation.

The next step in the investigation was to vary the conductivity of one of the materials and plot the change in attenuation and phase as a function of cladding thickness. Figures 11 and 12 are the results for silicon where the percentage change in attenuation is plotted with the percentage change in conductivity as a parameter. The curve indicates that for a proper choice of silicon thickness (.13 microns) the attenuation changes by approximately the same percentage as the conductivity. The phase characteristic (Figure 12) also shows an appreciable change for proper choice of silicon thickness. It is also interesting to note that maximum phase change occurs at the 0% crossing of the attenuation curve, which indicates a device could be designed as either an amplitude or phase modulator.

Based on these calculations several devices were constructed to verify the predicted attenuation variation with cladding thickness. It was hoped that these devices would not only verify

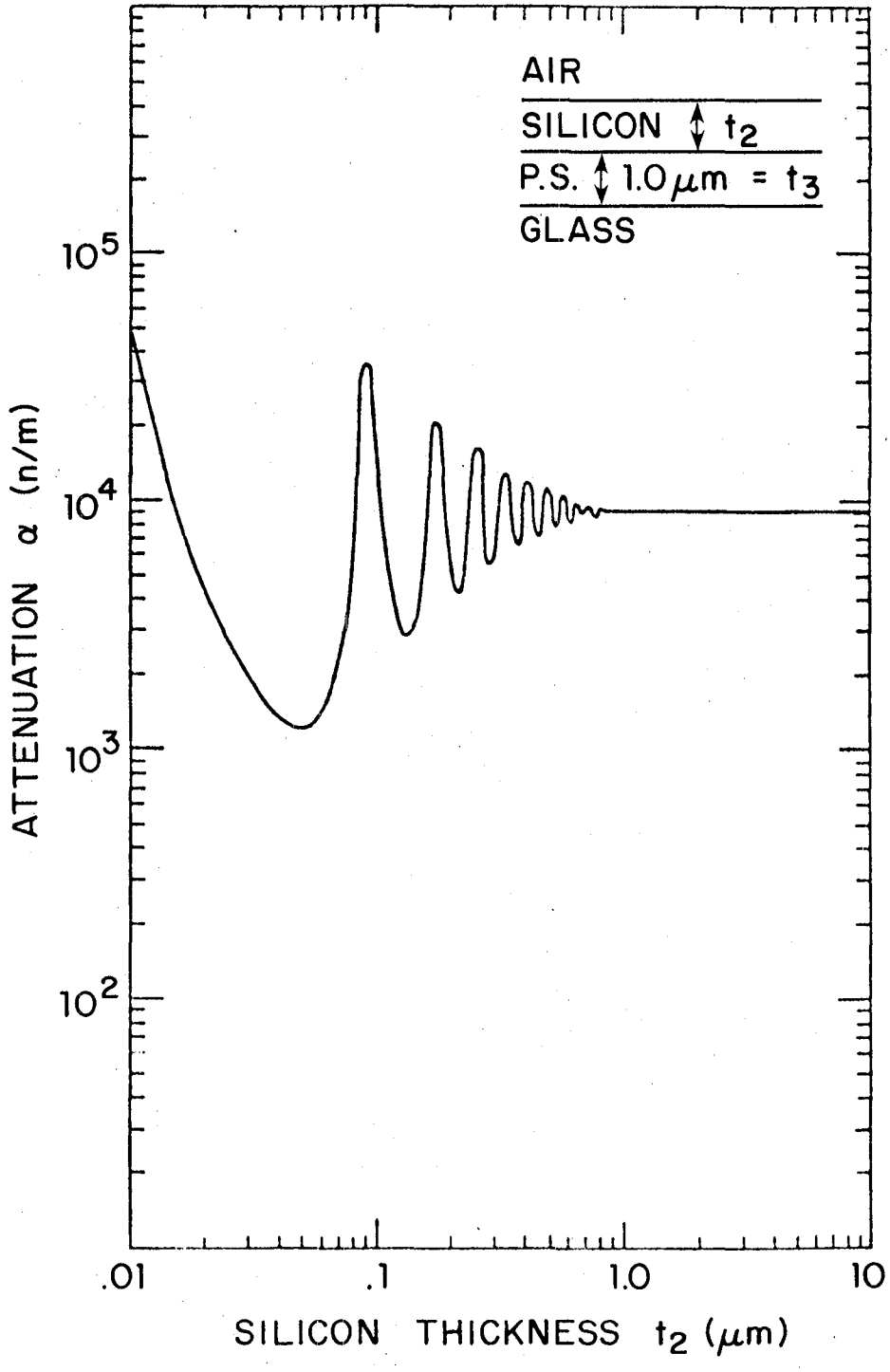

Figure 7. Silicon/Air Clad Guide Attenuation vs. t_2 (TE_o Mode, normal conductivity)

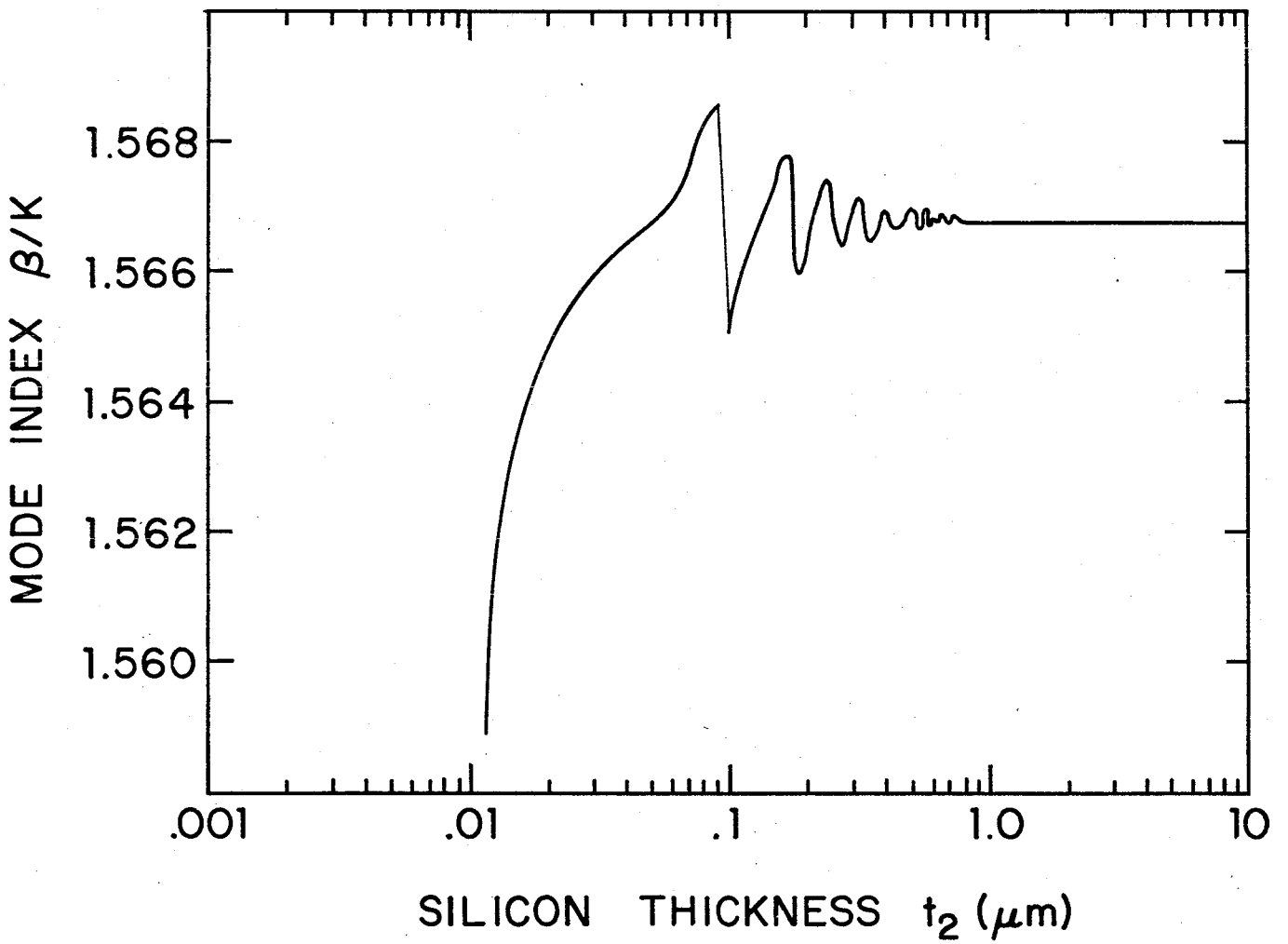

Figure 8. Silicon/Air Clad Guide β/κ vs. t_2 (TE_o Mode, normal conductivity)

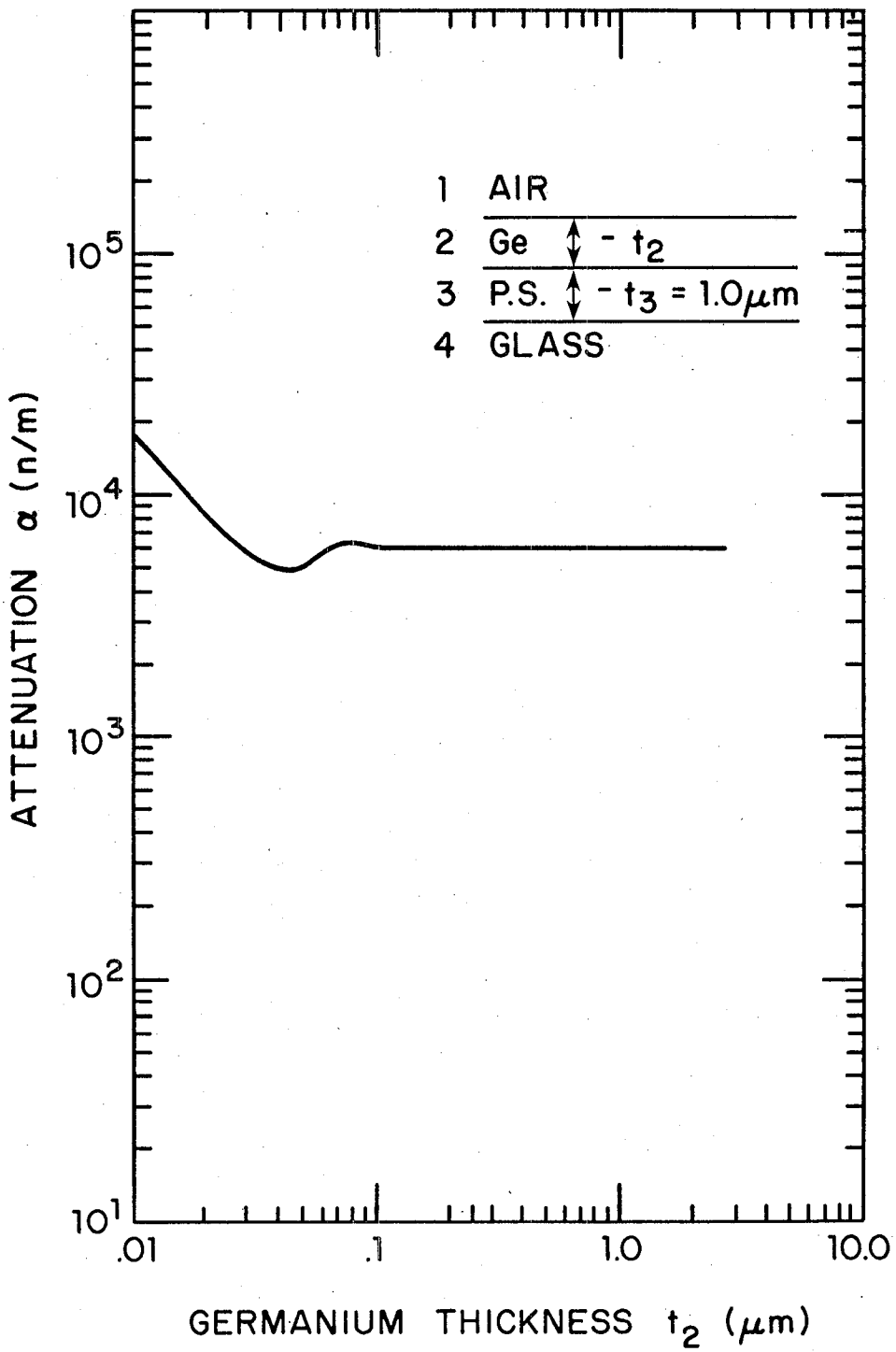

Figure 9. Germanium/Air Clad Guide Attenuation vs. t_2 (TE_o Mode, normal conductivity)

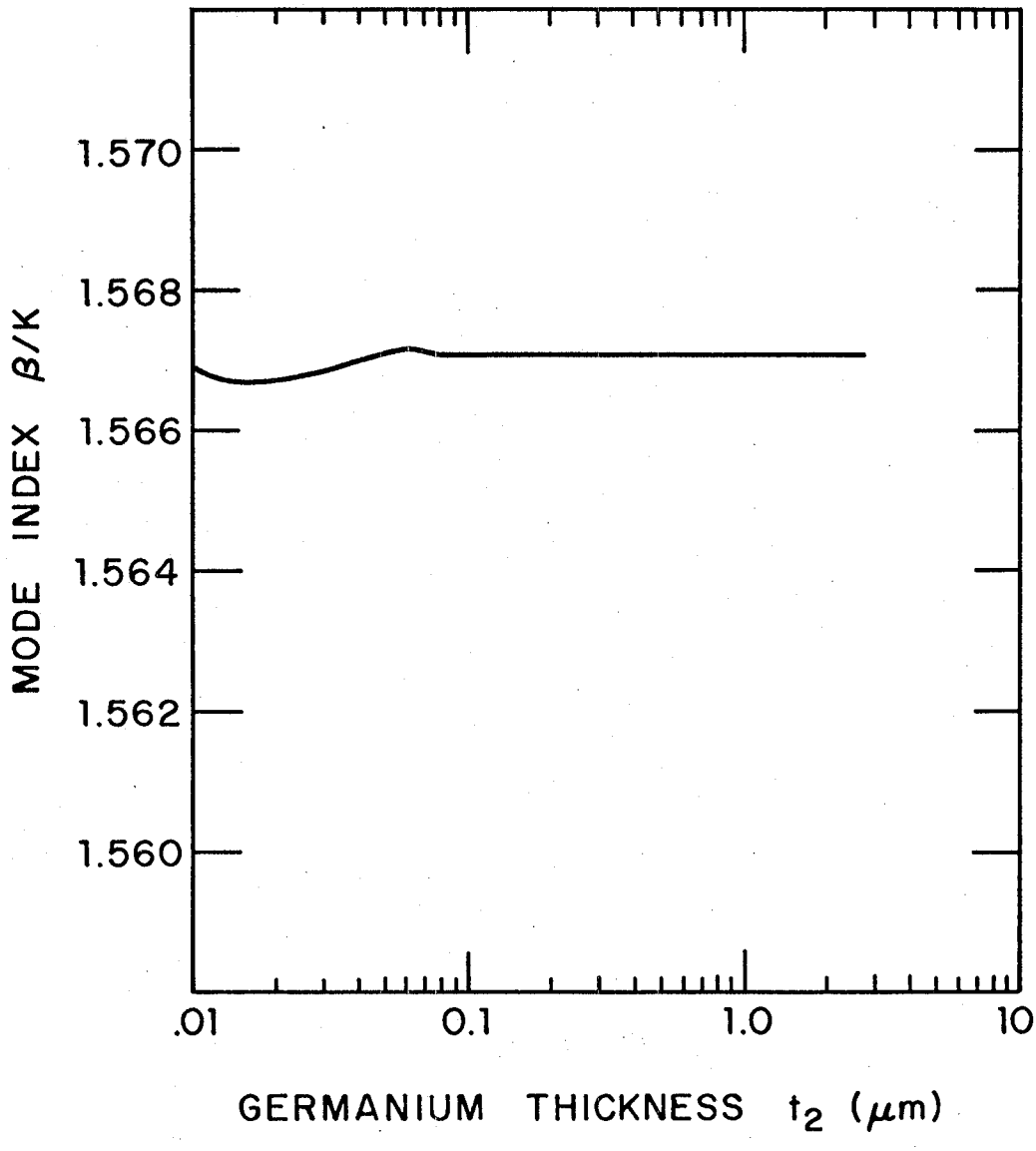

Figure 10. Germanium/Air Clad Guide, β/κ vs. t_2
(TE Mode; normal conductivity)

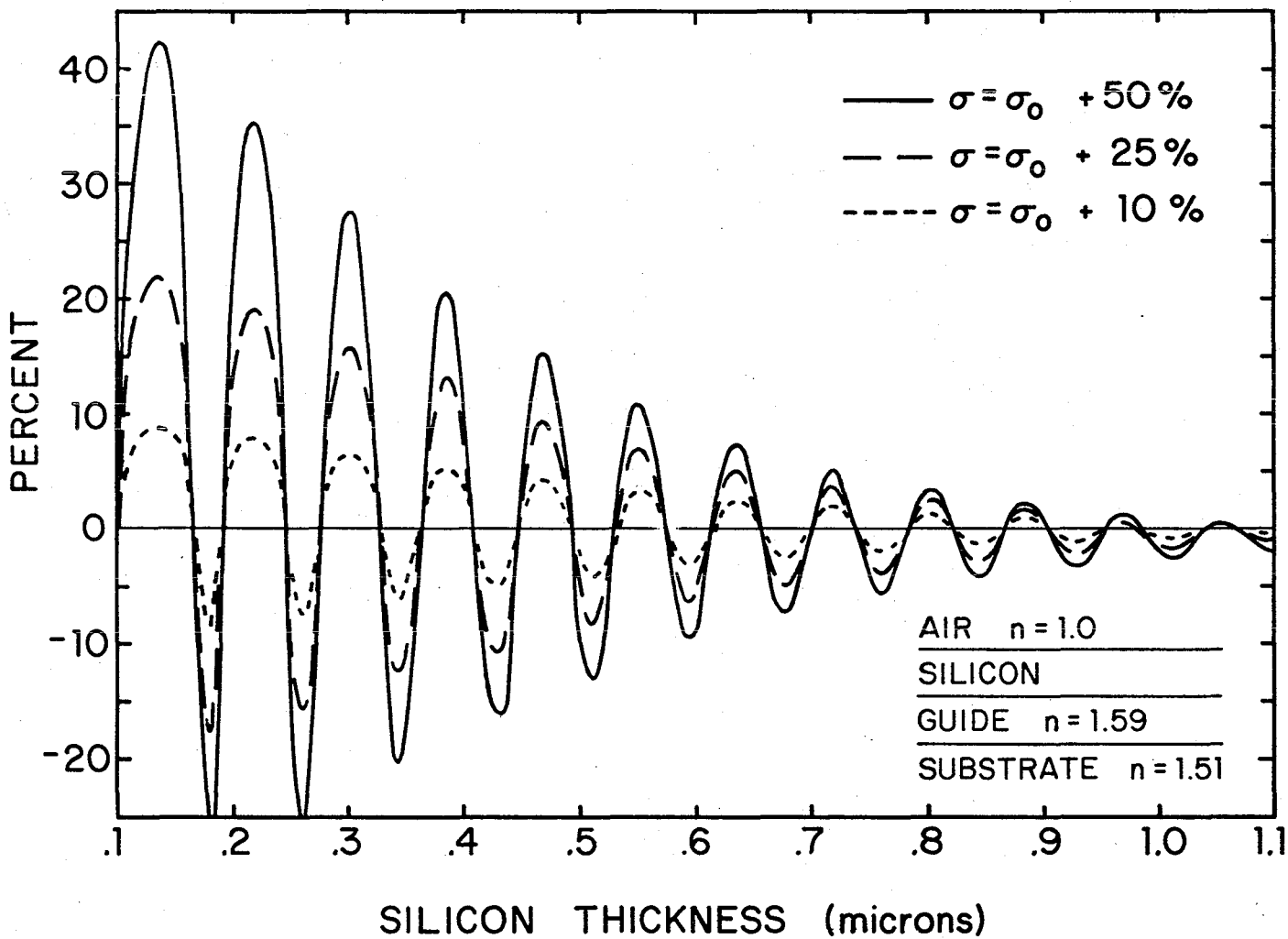

Figure 11. Calculated Percent Change in Attenuation Over Attenuation Calculated at 10 Micrometers Thickness for the TE_o Mode (t_3 = 1.0 μm).

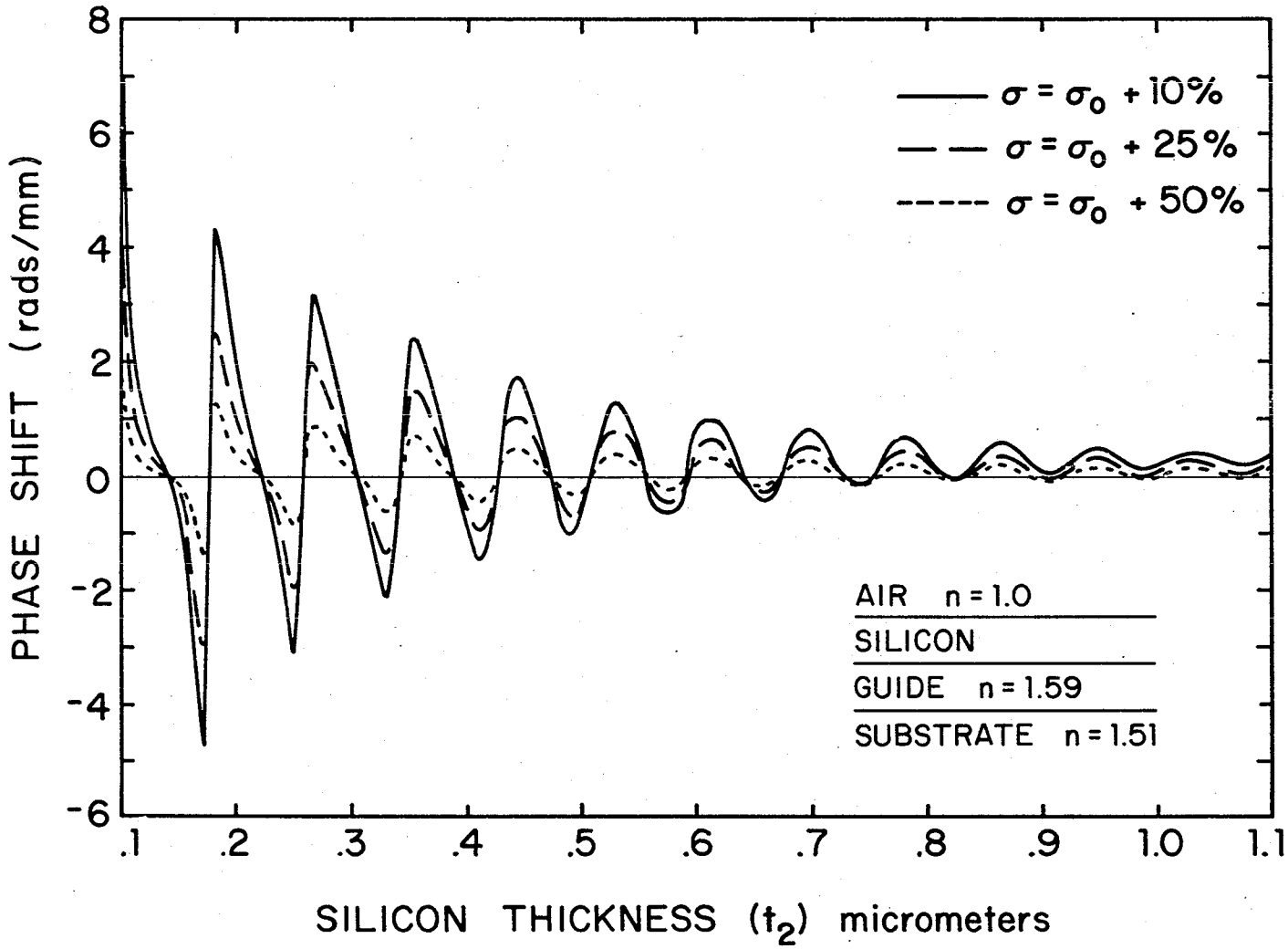

Figure 12. Calculated Relative Phase Shift Compared to that Calculated for a Silicon Thickness of 10 micrometers.

the calculations but prove that the magnitude of the effect was large enough for use as a modulator. Silicon was selected as the semiconductor to be deposited on the waveguide because of the well-developed deposition technology. Discussions with several people working with amorphous semiconductors indicated potential variation in the optical properties of these amorphous films with deposition method and temperature. Thus values of refractive index and loss coefficients used in our calculations may not be accurate for real films. After initial investigation of the two principal methods of deposition of amorphous silicon (CVD and e-beam evaporation) it was decided to use the e-beam technique because of better reproducibility in optical constant. The e-beam system at Cornell University, Materials Science Department, was used for our initial films.

The film thickness was selected based on the predicted attenuation and phase variations. A wedge shaped film varying in thickness from 0.1 to 1.0 micrometers was deposited with the Cornell system in the configuration shown in Figure 13. A detailed discussion of the deposition technique is available in reference 3. According to the predictions, the attenuation should vary by >900 dB over this thickness region and thus the effect would be readily observable.

This device was fabricated by first constructing an ion exchange waveguide (3) and then evaporating the silicon film on the waveguide through a mask. The silicon thickness gradient was obtained by evaporating through a wedge shaped oscillating shutter. Dektak measurements of the resulting films indi cated

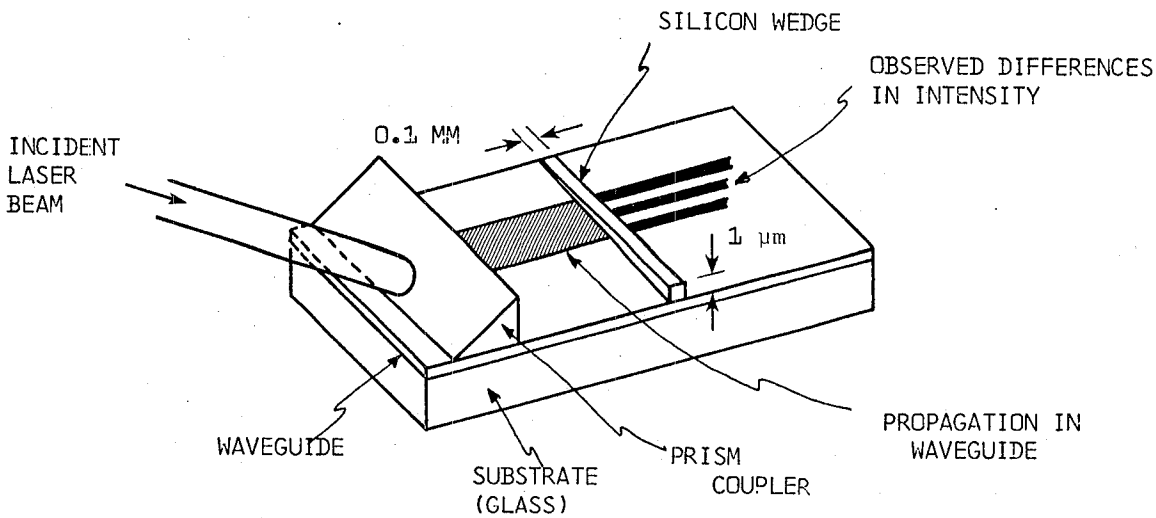

Figure 13. Experimental Device for Verification of Oscillations in Intensity.

a film thickness varying from .06 to .105 micrometers rather than the 0.1 to 1.0 desired. Measurement of the attenuation of the best of three guides fabricated was accomplished by coupling a laser beam into the waveguide through a prism coupler. The intensity of the guided beam was then measured with a photodetector and a liquid coupler before and after the silicon film giving the relative attenuation of the silicon film.

Due to the silicon film not being in the thickness range desired and problems with making repeatable measurement using the liquid coupling technique, the measured data was difficult to correlate with the predicted curves. Figure 14 shows the measured points obtained from two seperate sets of measurements of the guide. There appears to be a general decrease in the attenuation as the thickness approaches 0.105 micrometers but it is not a well defined curve. The predicted data indicated the attenuation should be increasing in this region. It was felt that there were two possible causes for the discrepancies between the measurements and the predictions. The first explanation was that an oxide layer of 300A had grown on the silicon thus reducing the film to (a thickness of) 300Å (to 750Å). This would make the experimental curve match the calculated curve in magnitude and shape. Calculation of oxide growth on bulk silicon indicates a 10-20Å layer should be present. Unless the thin film behaves differently from the bulk material or if there were an interaction at the glass silicon interface this 300Å change in thickness needed to match the data with predictions could not be justified. The second explanation was that the silicon film was contaminated by impurities in the silicon and in the vacuum

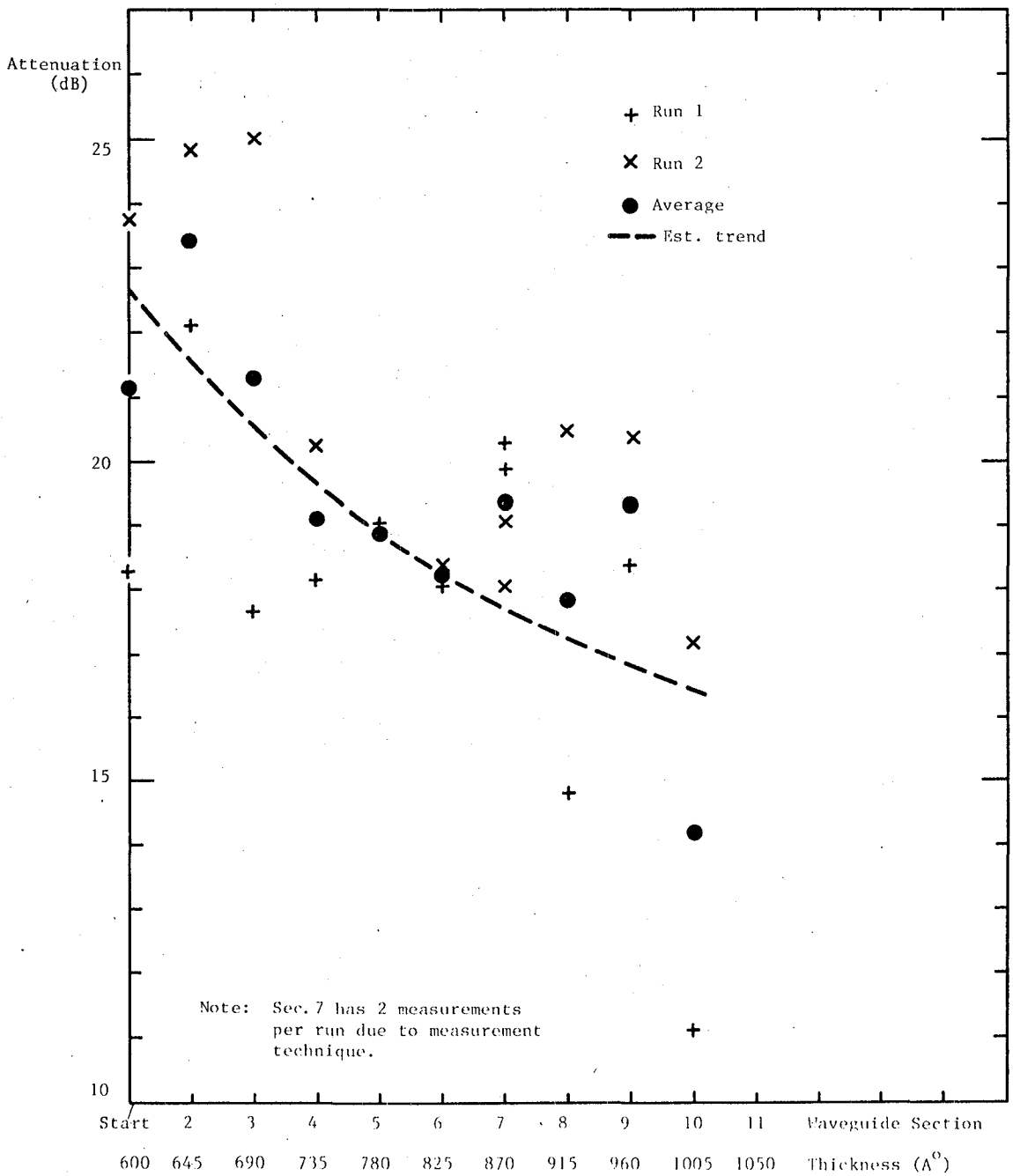

Figure 14. Experimental oc Measurements

chamber, thus changing the real part of the permittivity. A theoretical investigation of this second postulated effect is discussed in detail in section 3.

The work reported in the remainder of this report occurred from October 1980 to June 1981 and is an attempt to explain the origin of the effect. This work includes theoreticalanalysis, additional computer predictions and attempts at fabrication of improved experimental devices.

III. EFFECT OF CHANGES IN CLADDING PERMITTIVITY

Several explanations for the discrepency between experimental results and computer predictions were proposed. One possibility was that some changes had occurred in the real part of the permittivity of the silicon film from the value used in the computer calculations. Possible explanations for the permittivity change include mechanical irregularities in the Si film and inadvertent doping of the semiconductor layer.

Since the mechanisms for the ε' shifts were not well understood, a trial-and-error method was used to determine the value necessary to correlate experimental results with computer calculations. Initially, a $\Delta\varepsilon' = 16.76 - 15.76 = 1.0$ was used; however, the magnitude of the curve shift was insignificant. Further attempts were made and the results of the computer calculations are shown in Figure 15. Observe that the real part of the permittivity must change by at least 40% in order to produce an appreciable horizonal curve shift; however, the attenuation-thickness curve shifts vertically as well (the local minima shifts but the local maxima remains the same). In addition, a 40% decrease in the permittivity (from 16.76 to 10.76) only shifts the curve 200Å, unfortunately, a 500Å curve shift is necessary to achieve any kind of correlation between experimental results and computer calculations. This indicates that a permittivity decrease on the order of 80% would be necessary to achieve correlations; but, a permittivity decrease also shifts the magnitude of the local minima, and further correlation problems are

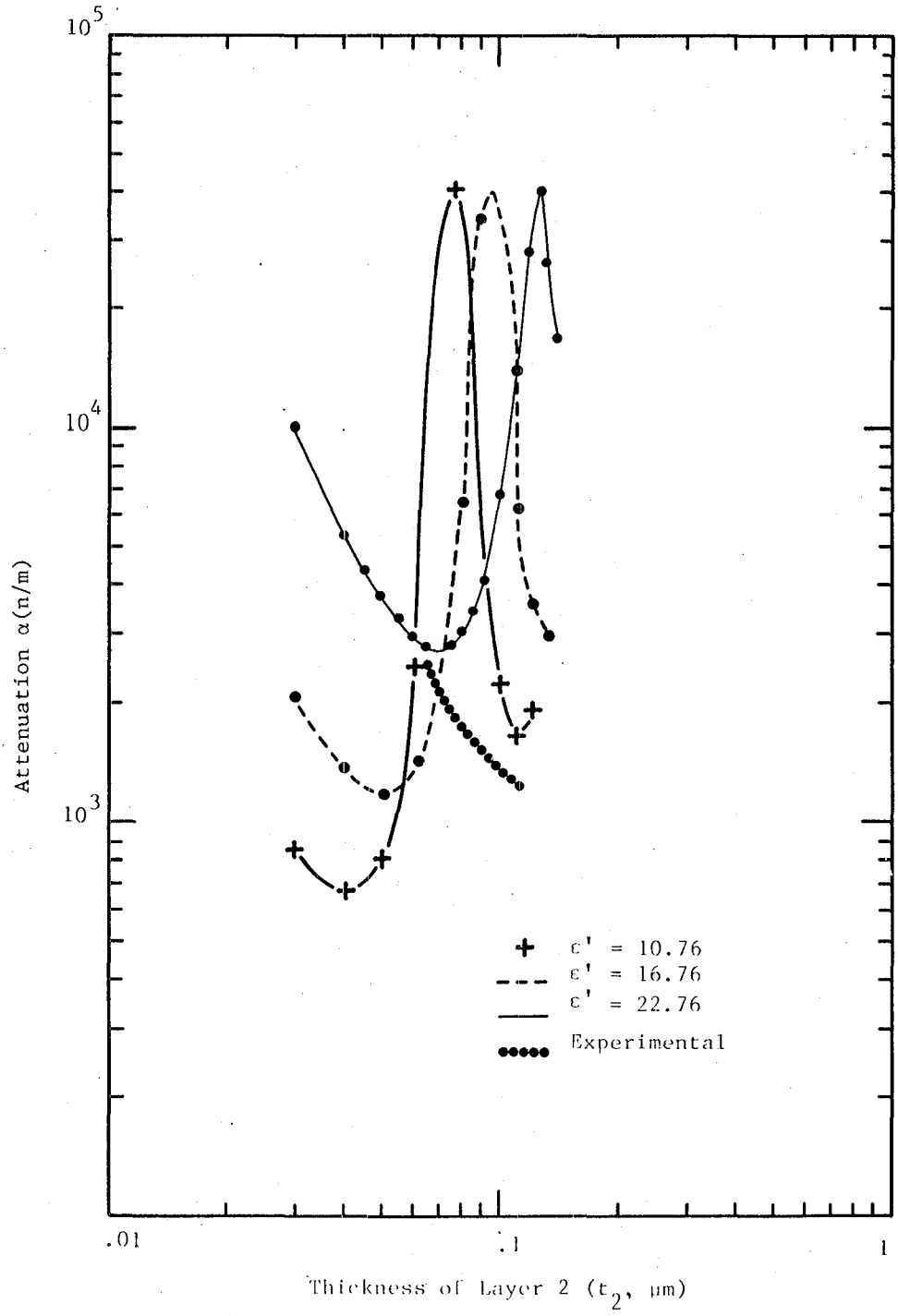

Figure 15. Relative Shift in Attenuation Peaks With Permittivity Changes.

introduced. It appears, then, that an ε' shift is not a suitable explanation for the discrepency between experimental results and computer predictions.

IV. ANALYSIS OF PREDICTED WAVEGUIDE CHARACTERISTICS

A. Theory

The damped oscillations of the attenuation-silicon thickness curves and the phase-silicon thickness curves can be explained in terms of both a ray-optics approach for light propagation in the waveguide and a careful analysis of the electric and magnetic fields of the propagating wave within the structure.

Heavens (8) considered a thin film of material with $n = 2$ and $k (k = \alpha\lambda/4\pi)$ varying and calculated the expected phase change on reflection of an incident wave at an air film surface. For k very small, the phase change oscillates, and for k large, the phase changes very little until the film thickness approaches zero. This behavior has also been predicted by Stratton (9) and is similar to the effect we have observed.

The proposed explanation for the results is that there isan interference effect across the waveguide and when constructive interference occurs in the semiconductor cladding, the propagating wave field strength will be greater and higher attenuation is expected. Likewise, destructive interference will cause a much lower attenuation. Normalized phase shifts must be at a maximum when the interference effects are at a minimum, similar to the results of transmission calculations of waves through an absorbing medium. Increasing the conductivity of the semiconductor cladding increases the field strength attenuation in the cladding which decreases the effect of the interference. At the points where a greater conductivity causes a lower attenuation, the greater conductivity increases the reflection at the cladding-core interface, and thus there is less field

strength in the absorbing medium and less attenuation in the propagating wave.

Accurate electric and magnetic field plots of the wave within the structure were obtained by using program MODEIG (6) and confirm the validity of this argument. Program MODEIG obtains a 2 x 2 characteristic matrix of Maxwell's equations and boundary conditions for each waveguide layer defined as:

$$C_\ell = \begin{bmatrix} \cos \sigma_\ell + (i\, Y_x) \sin \sigma_\ell \\ + (i\, Y_x) \sin \sigma_\ell \cos \sigma_\ell \end{bmatrix}$$

where $\sigma_\ell = K_\ell \tau_\ell$ (the complex phase thickness of the layer)

$$\kappa_\ell^2 = \omega_r^2 \mu_r \varepsilon_r - \left(\frac{K_z}{K_o}\right)^2$$ (the complex propagation constant of the layer)

Y_x = generalized parameter of the field distribution within the layer

Through a complex series of multipications, of the above characteristic matrix for each layer, the propagation constant andthe incremental field distributions within the structure are calculated. From the characteristic matrix, we observe that the field distribution in each waveguide layer is a complicated trigonometric function of the complex propagation constant, . For a lossless structure, however, the wave function profile for each layer is effectively reduced from its complicated matrix

representation to the following:

$$\phi_i = e^{j(\omega t - K_z z)} \begin{cases} A_y e^{-\sigma_4} & i = 4 \\ A_3 \cos(\sigma_3 + \Psi) & i = 3 \\ A_2 \cos(\sigma_2 + \delta) & i = 2 \\ A_1 e^{\sigma_1} & i = 1 \end{cases}$$

We again note a trigonometric variation in the semiconductor cladding and dielectric guide, and a decaying exponential in the semi-infinite layers.

B. Calculated Field Distributions

We now consider the problem of correlating the local maximum/minimum points on the attenuation-silicon thickness curve with the electric and magnetic field distributions at the appropriate thickness. Results from program MODEIG indicate that the presence of a thin silicon film (<100Å) has little effect on the wave function profiles; the profiles are very similar to those of the three-layer structure. For the thick silicon film structure, however, the lowest order mode of the lossless three-layer structure appears to couple to the modes assosciated with the semiconductor-dielectric interface. Furthermore, the coupling between the modes supported by the three-layer lossless structure and the modes associated with the semiconductor-dielectric interface determines the attenuation of the complete four-layer structure.

The real part of the wave function profile in the transverse direction for the TE_o mode is shown for a cladding thickness, t_2 =.007 μm (Figure 16). We note that the thin silicon film does not appreciably affect the wave function profile of the TE_o mode.

For the first local minimum (t_2 = .05 μm), we observe that the field strength at the silicon-dielectrc interface approaches zero (Figure 17). We also note the expontially decaying solutions in the outer, semi-infinite layers.

For t_2 = .09 μm (the first local maximum), we observe a sharp peak in the wave function profile at the silicon-dielectric interface (Figure 18).

Similar behavior is noted for the next local minimum/maximum pair (t_2 = .13 μm and t_2 = .18 μm) (Figure 19 and Figure 20). The field strength is effectively zero at the silicon-dielectric interface for the local minimum, and a sharp peak in the wave function at the interface is evident for the local maximum. We also note an increase in the number of field oscillations in the semiconductor cladding.

Again, for the next local minimum/maximum pair (t_2 = .22 μm and t_2 = .26 μm) (Figure 21 and Figure 22) we observe an increase in the number of field oscillations in the silicon and a corresponding increase or reduction in field strength at the silicon-dielectric interface. Interestingly enough, at the local maximum (t_2 = .26 μm) the field in the dielectric guide decays rapidly to zero, and the field strength is at a maximum at the silicon-dielectric interface. This behavior was not evident for the other local maxima (t_2 = .09 μm and t_2 = .18 μm). A considerable field strength was, of course, apparent at the interface; how-

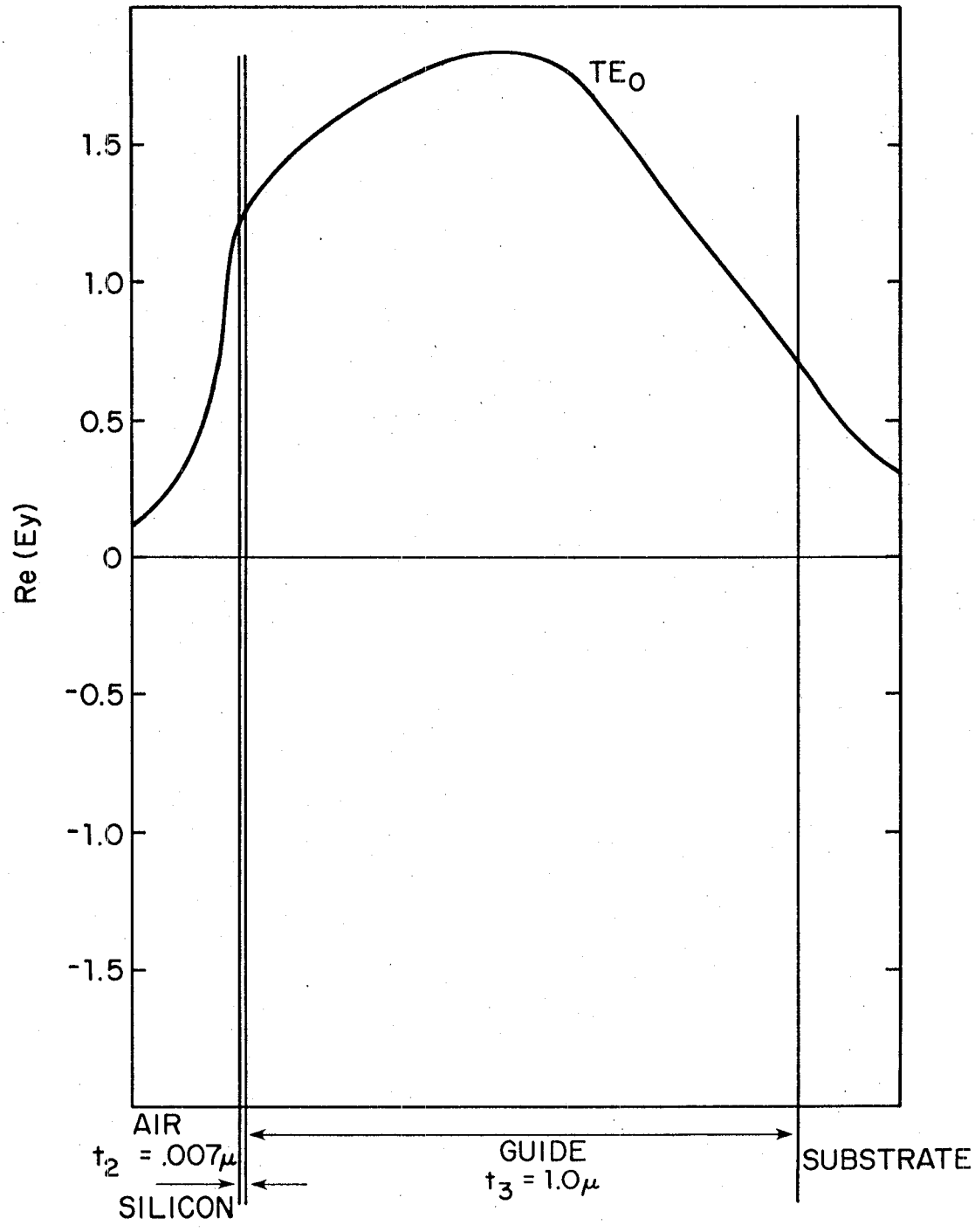

Figure 16. Wave Function Profile (t_2 = .007 μ)

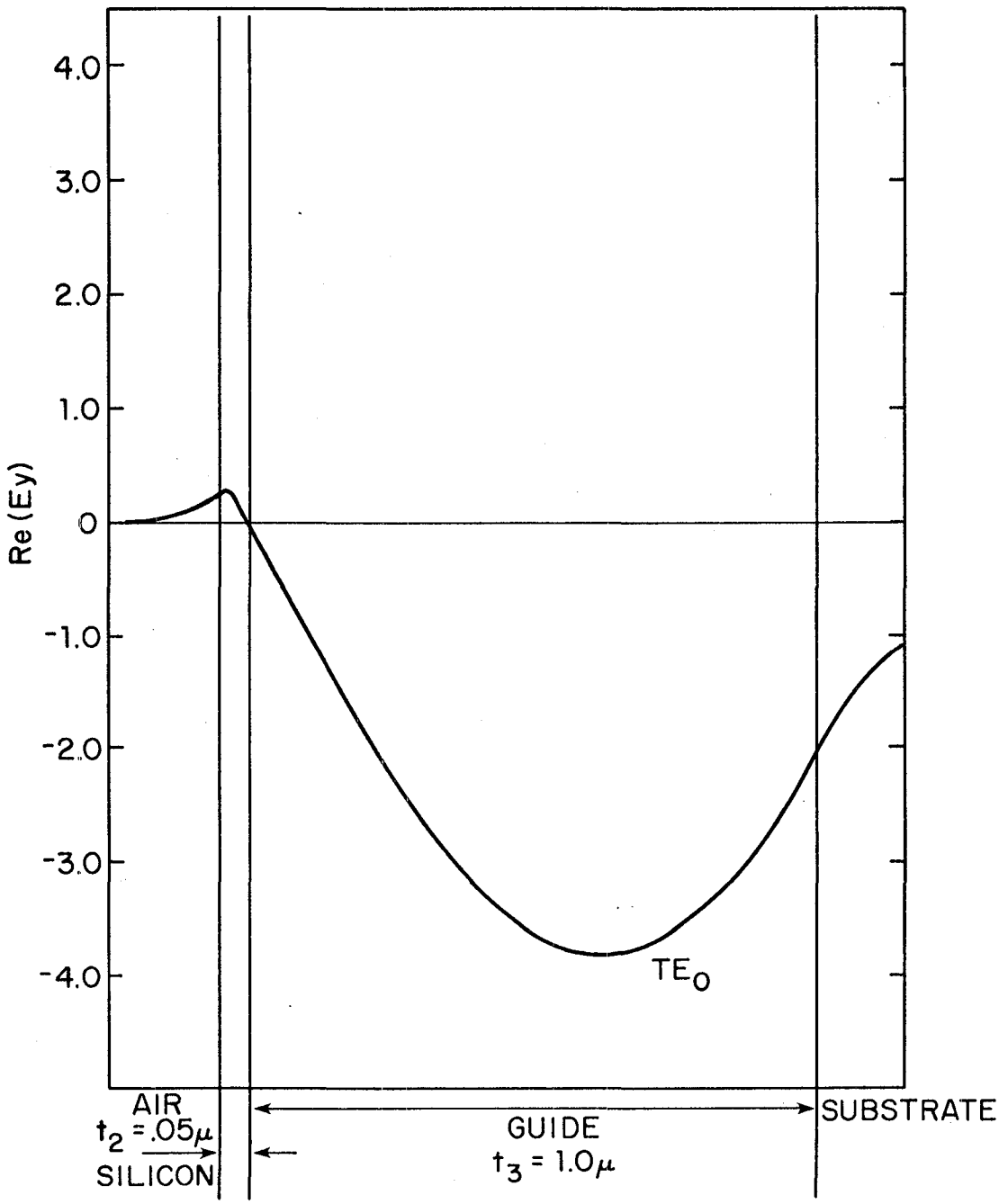

Figure 17. Wave Function Profile (t_2 = .05 μ, local minimum)

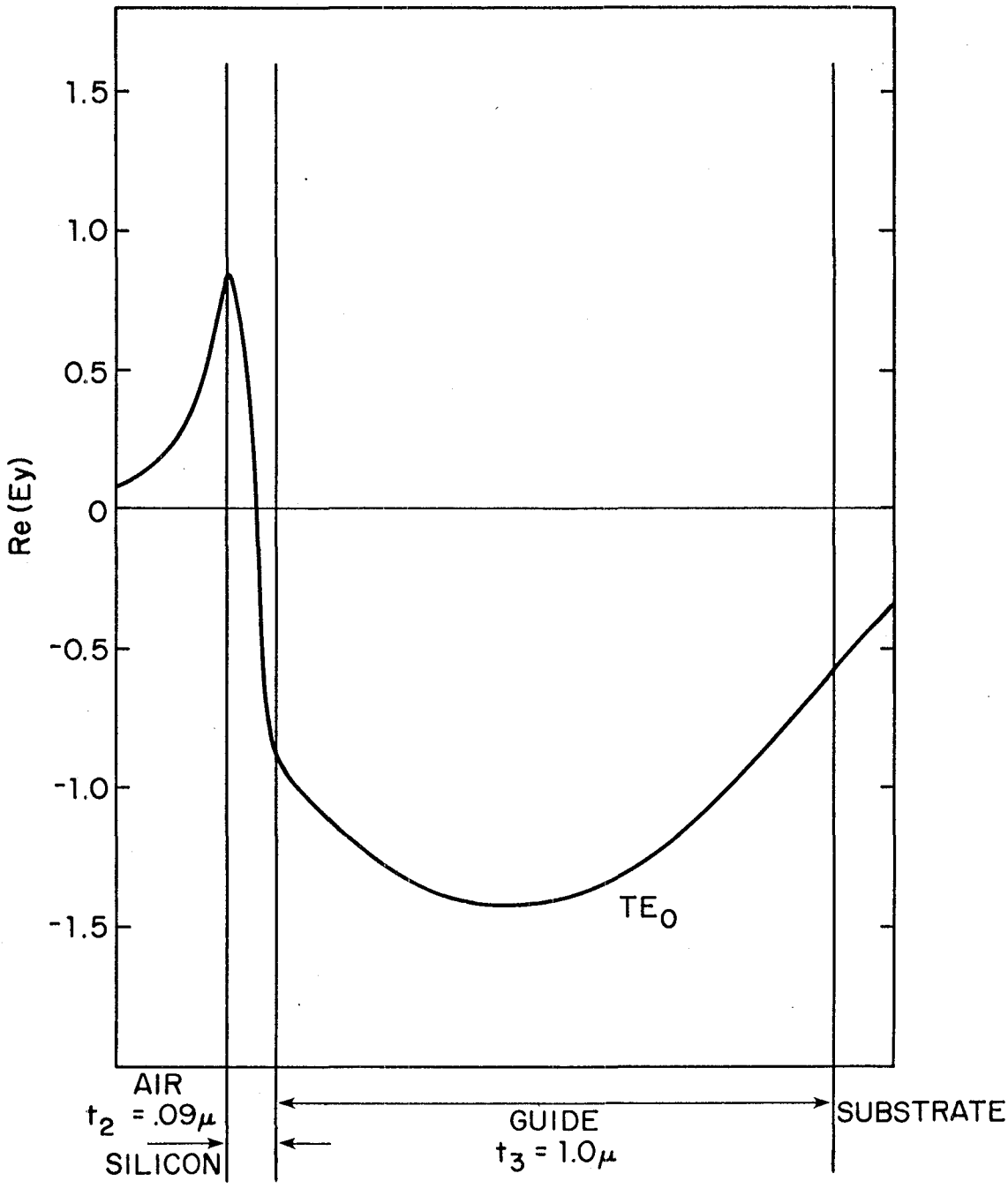

Figure 18. Wave Function Profile (t_2 = .09 μ, local maximum)

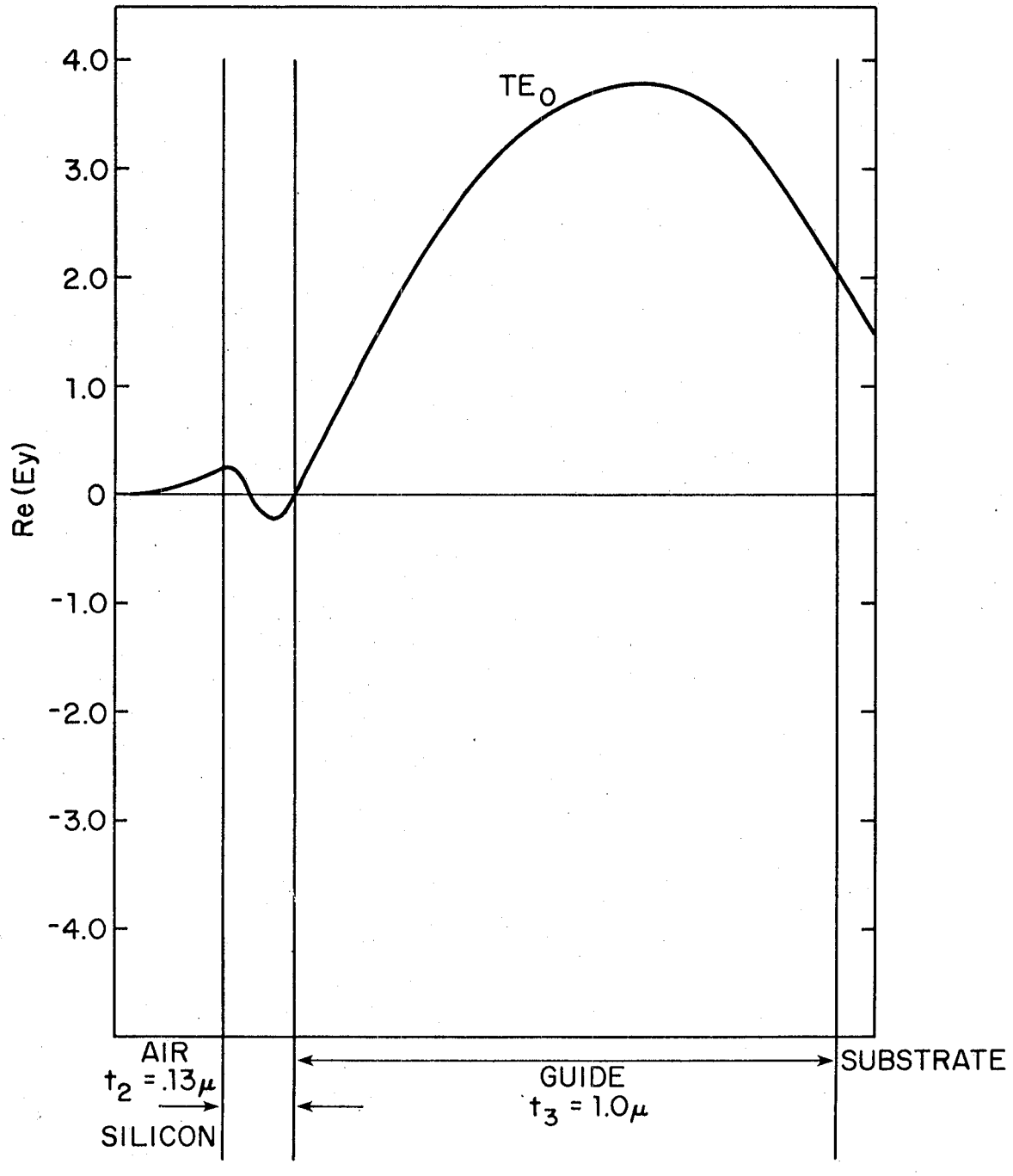

Figure 19. Wave Function Profile (t_2 = .13 μ, local minimum)

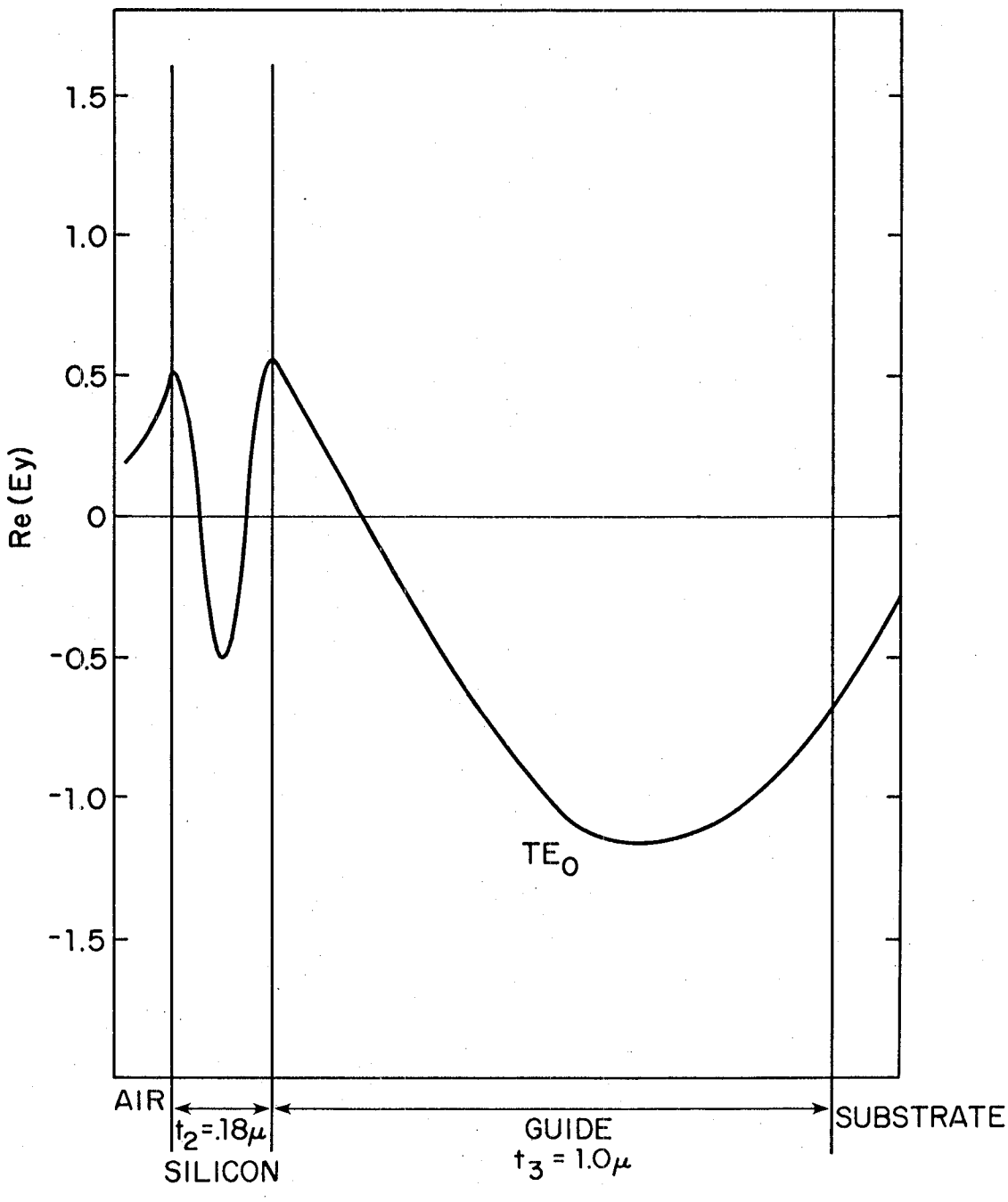

Figure 20. Wave Function Profile (t_2 = .18 μ, local maximum)

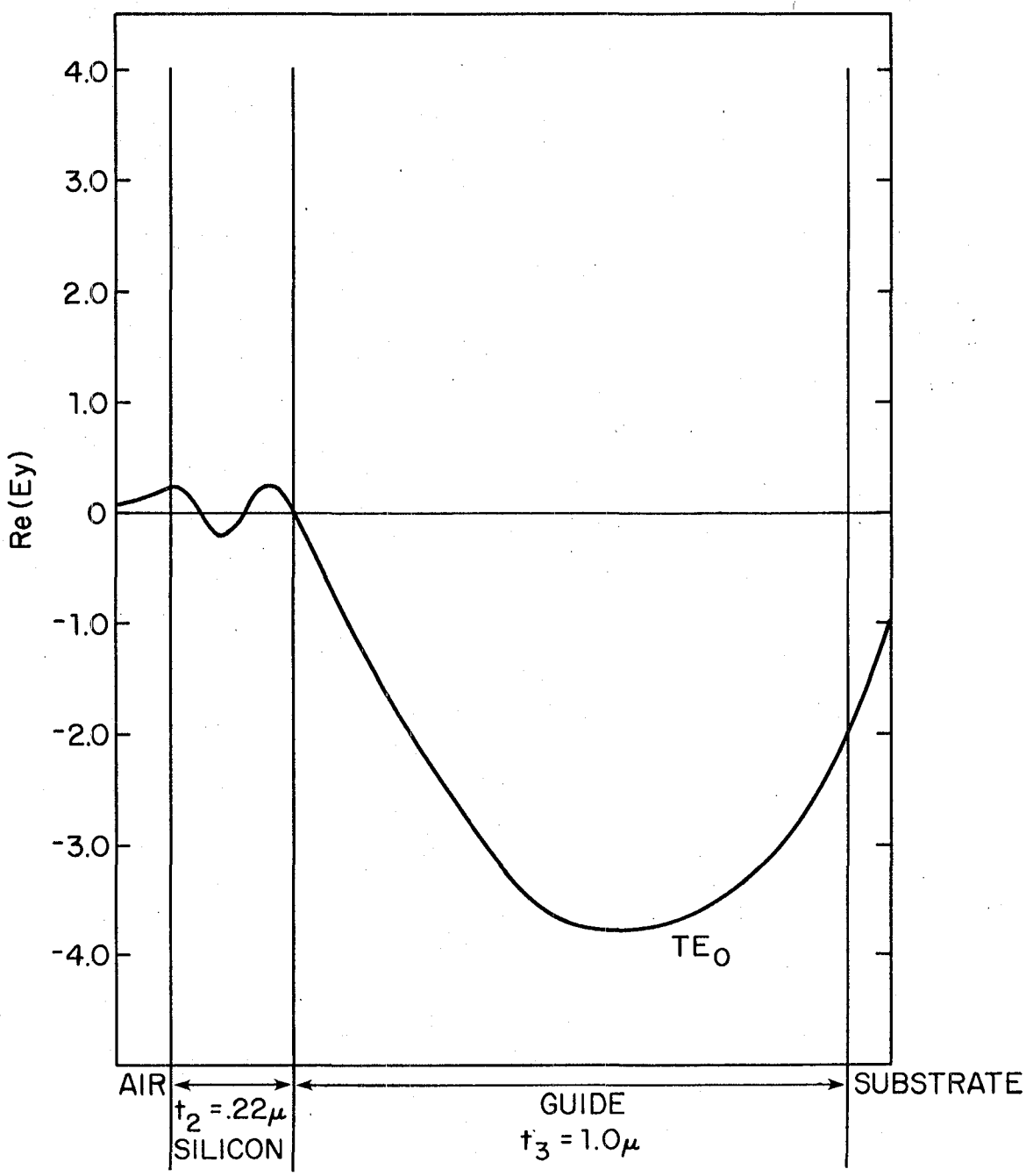

Figure 21. Wave Function Profile (t_2 = .22 μ, local minimum)

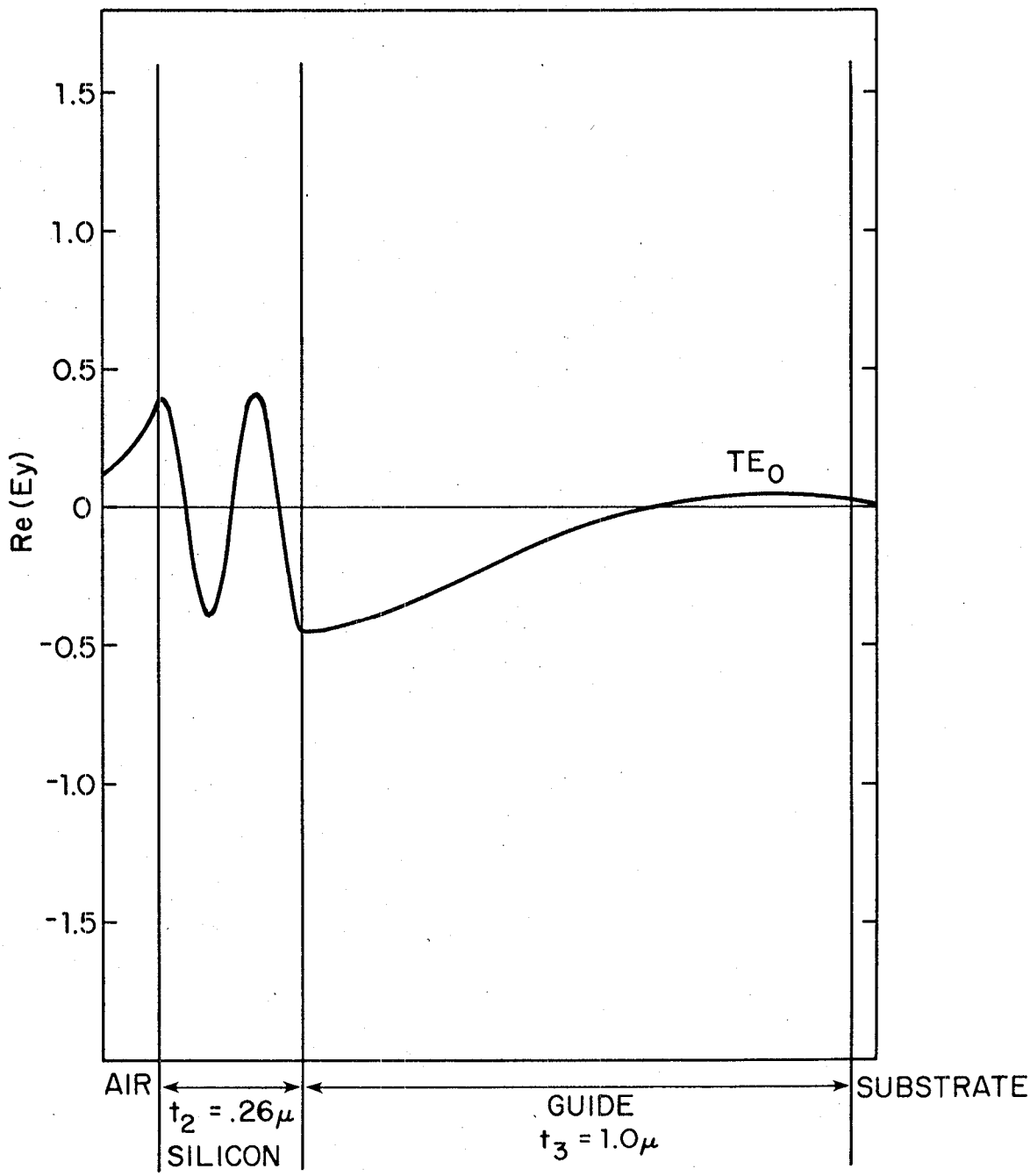

Figure 22. Wave Function Profile (t_2 = .26 μ, local maximum

ever, a sizable field was still noted in the dielectric guide. Consequently, fields were calculated at two thicknesses (t_2 = 0.255μm and t_2 = 265μm) on either side of t_2 = 0.26μm. For these two thicknesses we observe that there is, again, a sizable field contribution in the dielectric guide (Figure 23 and Figure 24). This result, in particular, indicates that the local "maxima" used for the computer calculations are not, precisely local maxima. Time and monetary constraints prevented more accurate determination of the local maxima points; however, appropriate field distributions for these thicknesses are still apparent.

The field plots indicate that the attenuation of the four-layer structure may be explained quite simply as a coupling between the basic three-layered waveguide (air-guide-substrate) modes and the surface wave mode supported by the silicon-dielectric interface. For a thin silicon cladding (.007μm) the wave function is not appreciably distorted and is everywhere positive which is appropriate behavior for the TE_0 mode. For a local minimum on the attenuation-silicon thickness curve, the field at the semiconductor-dielectric interface is zero, and for a local maximum, a considerable field is set-up at the interface which decays rapidly through the guiding region and the semi-infinite substrate. Furthermore, we note that the number of field oscillations in the silicon cladding is related to the silicon thickness and consequently to the order of the local maxima/minima points (first, second, third, etc.).

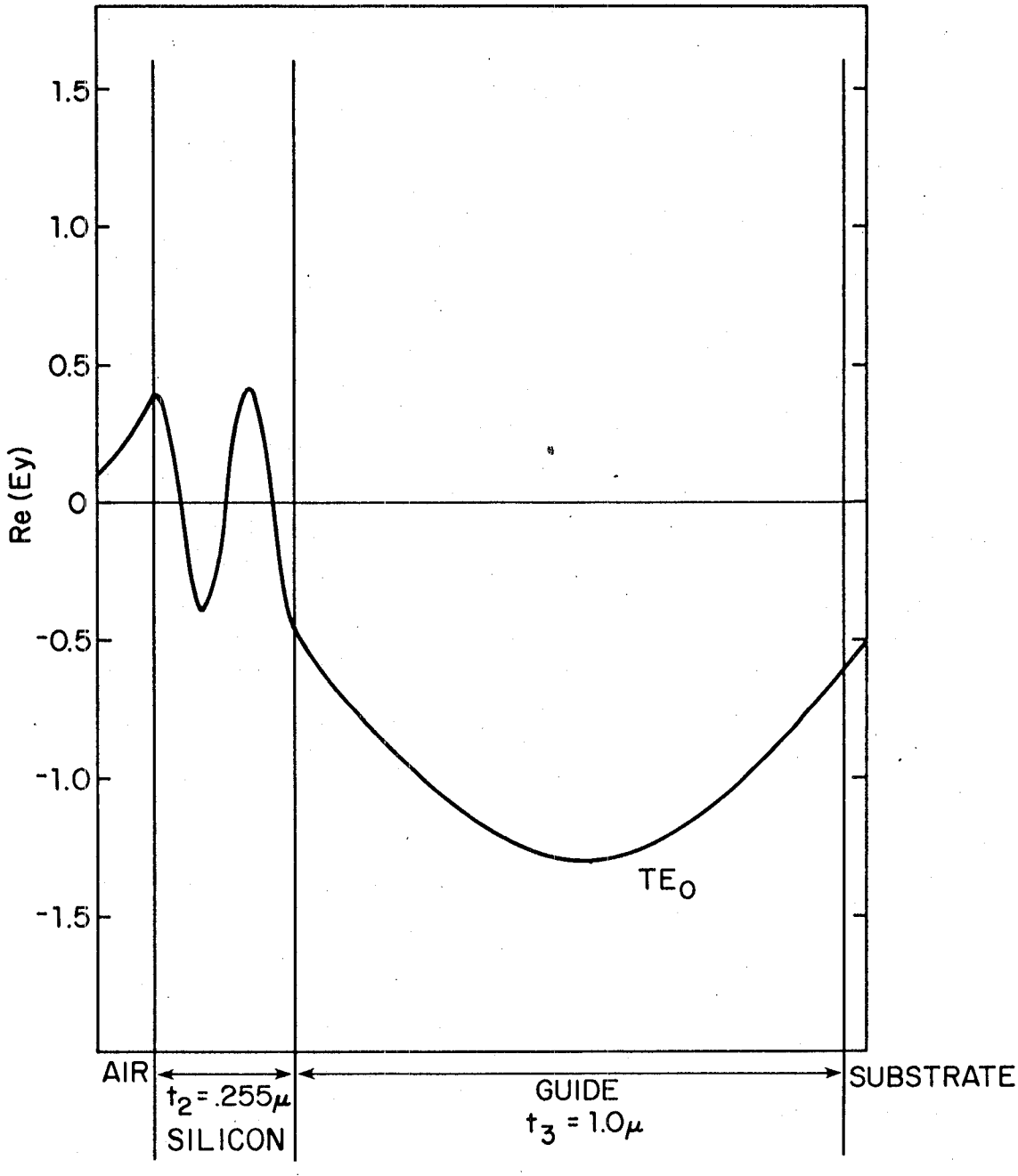

Figure 23. Wave Function Profile (t_2 = .255 μ, local maximum)

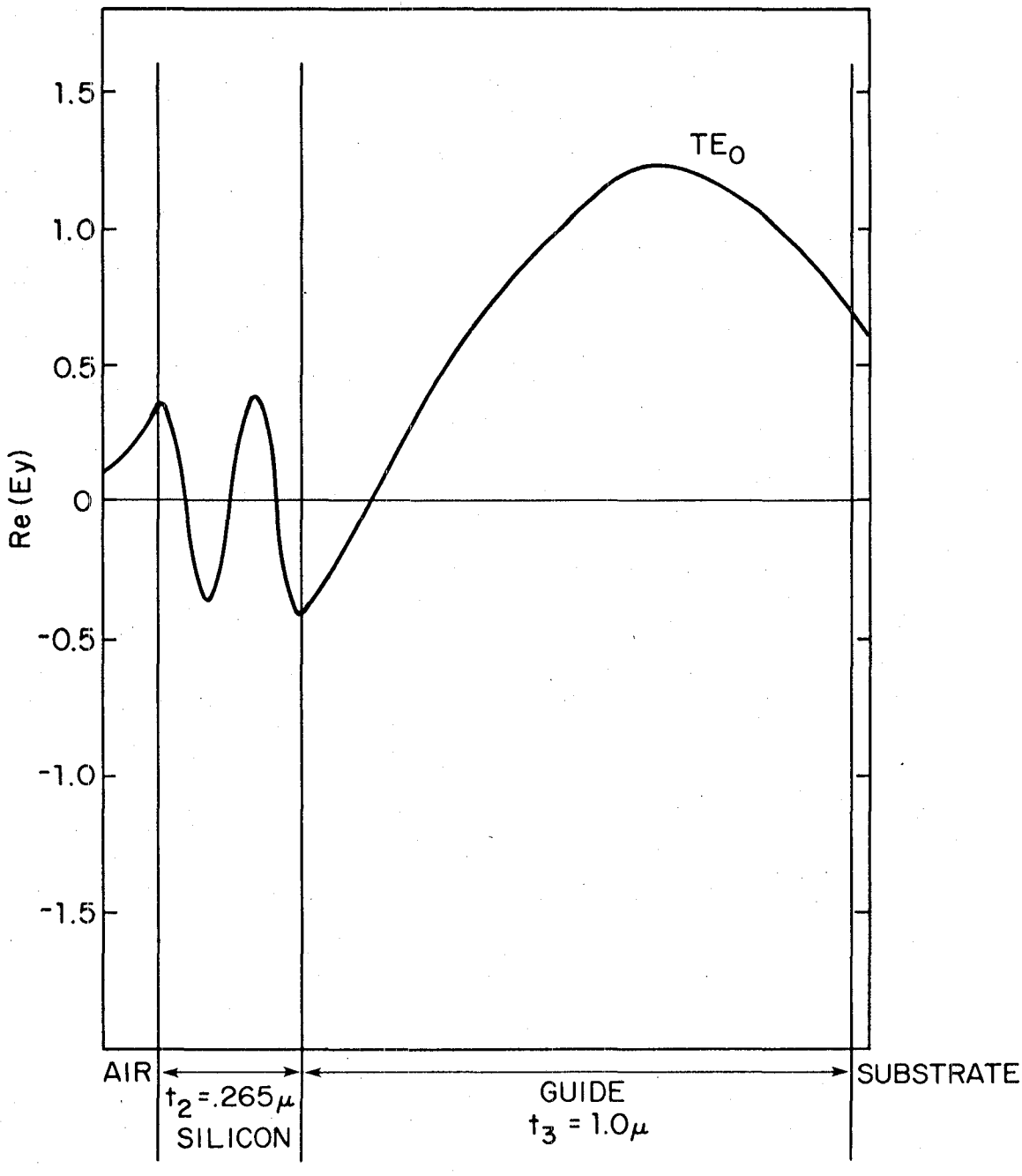

Figure 24. Wave Function Profile (t_2 = .265 μ, local maximum)

We recall that the wave function profiles in layers 2 and 3 are trigonometric for the lossless case. Indeed, the structure of interest is not lossless, so a slight distortion from the idealized trigonometric profiles appears. By solving for the TE_o mode of the four-layer structure we are requiring one half-cycle for the wave function profile in the guide; however, by progressively increasing the silicon thickness we are obtaining more oscillations for the trigonometric profile variation within the semiconductor. If the silicon thickness is such that the profile can go through exactly one cycle (or an integer multiple) we have perfect coupling at the silicon-dielectric interface and a minimum of the attenuation-silicon thickness curve; however, if the thickness is such that the wave function profile goes through half-cycle multiples, we observe a maximum on the attenuation-thickness curve. We note, of course, a slight distortion from the pure trigonometric variation in the silicon because boundary conditions must be matched at the appropriate interfaces. Furthermore, we observe that the direction of the field (positive or negative) in the dielectric is dependent on the tangent of the profile in the semiconductor (see t_2 = .255, .260, .265 μm). Finally, we note that the period of the attenuation-thickness curve (.08μm) is approximately identical to the half-period of the sinusoidal wave variation in the silicon cladding. A slight discrepenecy occurs, of course, as the silicon thickness is varied and the propagation constant, $\kappa_2 = \omega^2 \mu\varepsilon_2 - (K_z/k_o)^2$ for the silicon layer changes slightly; consequently, the period of the oscillations of the attenuation curve is not always 8 nanometers.

The effect that we have described is quite similar to certain developments in the theory of grating couplers (6, 10, 11, 12, 13). These results indicate that for some configurations (the grating layer placed between a surface guide and a high index substrate), the coupling efficiency is very dependent upon the grating period and guide thickness. For some combinations of parameters, the coupling efficiency could be large, but for other slightly changed values, the efficiency could become essentially zero. In reference (6) the authors state that these effects can be described as periodic coupling between the guided mode and other leaky modes of the same guide. Thus, if β_1 is the propagation constant for the bound mode, and β_2 is the real part of the propagation constant for a leaky mode then strong coupling to the radiated beam (from the leaky mode) can be expected when the phase matching condition is satisfied, $K = 2\pi/\Lambda = |\beta_1 - \beta_2|$, where Λ is the grating period.

In summary then, our results indicate that the damped oscillations of the attenuation-silicon thickness curve can be explained both in terms of a ray-optics approach for light propagation and in terms of a careful analysis of the electric and magnetic fields within the waveguide. Both approaches yield identical conclusions.

V. REDUCTION IN ATTENUATION: FIVE-LAYER STRUCTURES

Thin dielectric buffer layers have been used to lower the attenuation losses of metal-clad dielectric waveguides (14). These layers are placed between the dielectric core and the metal, and act as buffers to remove a large portion of the field from the metal claddings.

The effect of an SiO_2 buffer layer on the attenuation - Si thickness characteristics will be considered. Where an SiO_2 layer has been added between the guiding region and the semiconductor cladding to reduce the attenuation.

Using program MODEIG, five different cases were studied. They are:

Case
- i. verification of known results (convergence to three and four layer cases for $t_{SiO_2} = \infty$ and $t_{SiO_2} = 0$)
- ii. (α) vs Si thickness for different SiO_2 thicknesses ($\varepsilon_R = 2.12$)
- iii. (α) vs Si thickness for different SiO_2 thicknesses ($\varepsilon_R = 2.387$)
- iv. (α) vs Si thickness for different SiO_2 pemittivities (SiO_2 thickness = 1000$\mathring{A}$)
- v. (α) vs Si thickness for different SiO_2 permittivities (SiO_2 thickness = 2000$\mathring{A}$)

Case i

The attenuation constant (α) vs Si thickness is plotted for an SiO_2 (ε_R = 2.12) thickness of 100Å (Figure 25). The attenuation-Si thickness curve for the simple four-layer structure is shown for reference. Note that the attenuation-Si thickness curve for an SiO_2 thickness of 100Å converges to the simple four-layer case, which is, at least, intuitively correct.

Further computer modeling studies indicate that the attenuation-Si thickness curve converges to the lossless three-layer case for $t_{SiO_2} > 2000$Å and that the attenuation constant (α) can be effectively reduced to zero with large buffer layer thicknesses.

Case ii

The attenuation constant (α) vs Si thickness is plotted for two different SiO_2 (ε_R = 2.12) thicknesses (1000 and 2000Å) Figure 26. The attenuation-Si thickness curve for the simple four-layer structure is shown for reference. The familiar damped sinusoidal behavior is apparent for all buffer layer thicknesses (100, 500, 1000 and 2000Å). Most importantly, the attenuation can be reduced significantly with the addition of the SiO_2 buffer layer while still preserving the damped sinusoidal behavior of the attenuation-Si thickness curve. The percentage decrease in attenuation (relative to the four-layer values) for different buffer layer thicknesses is summarized below.

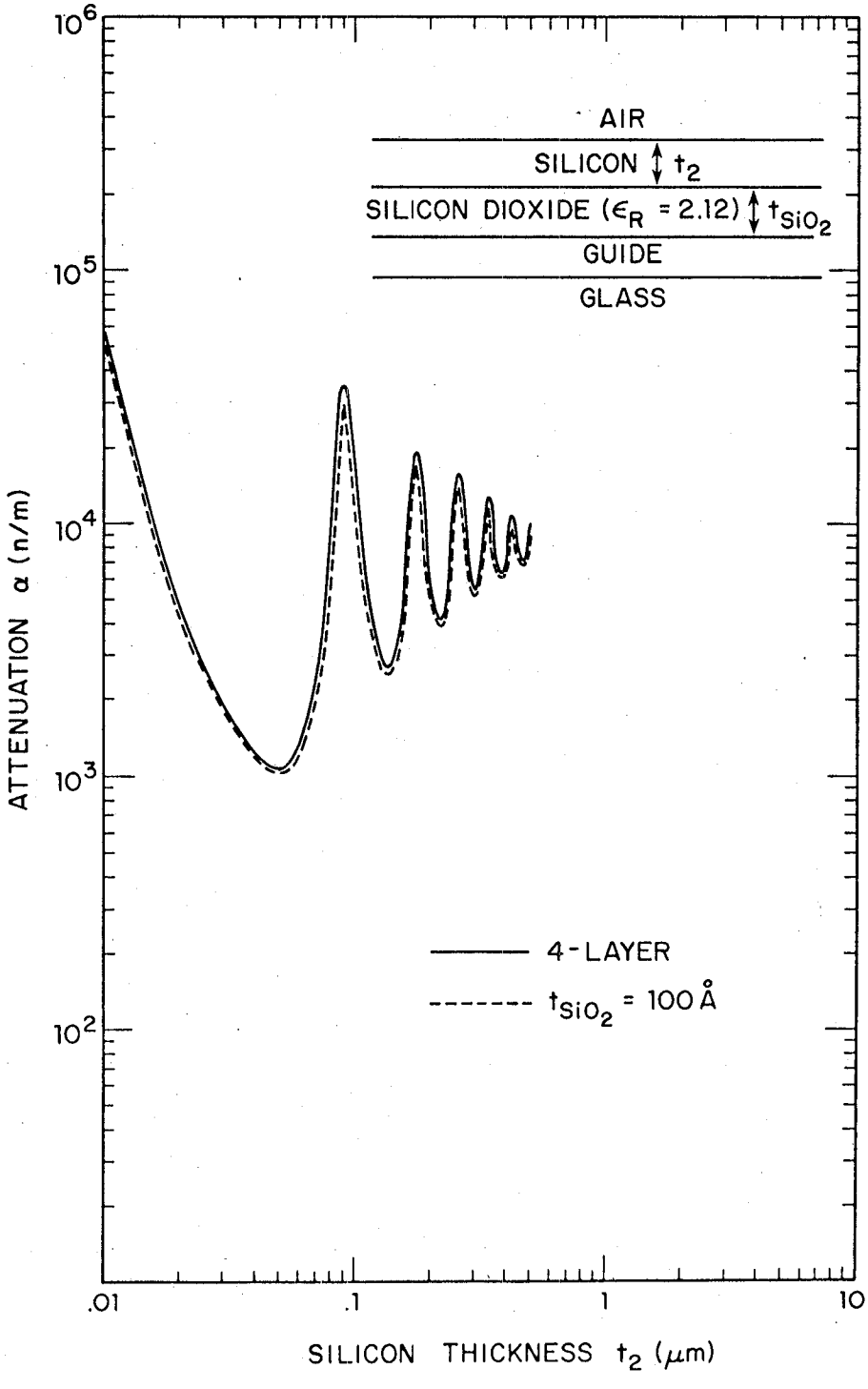

Figure 25. Attenuation Characteristics for 5-layer Structure

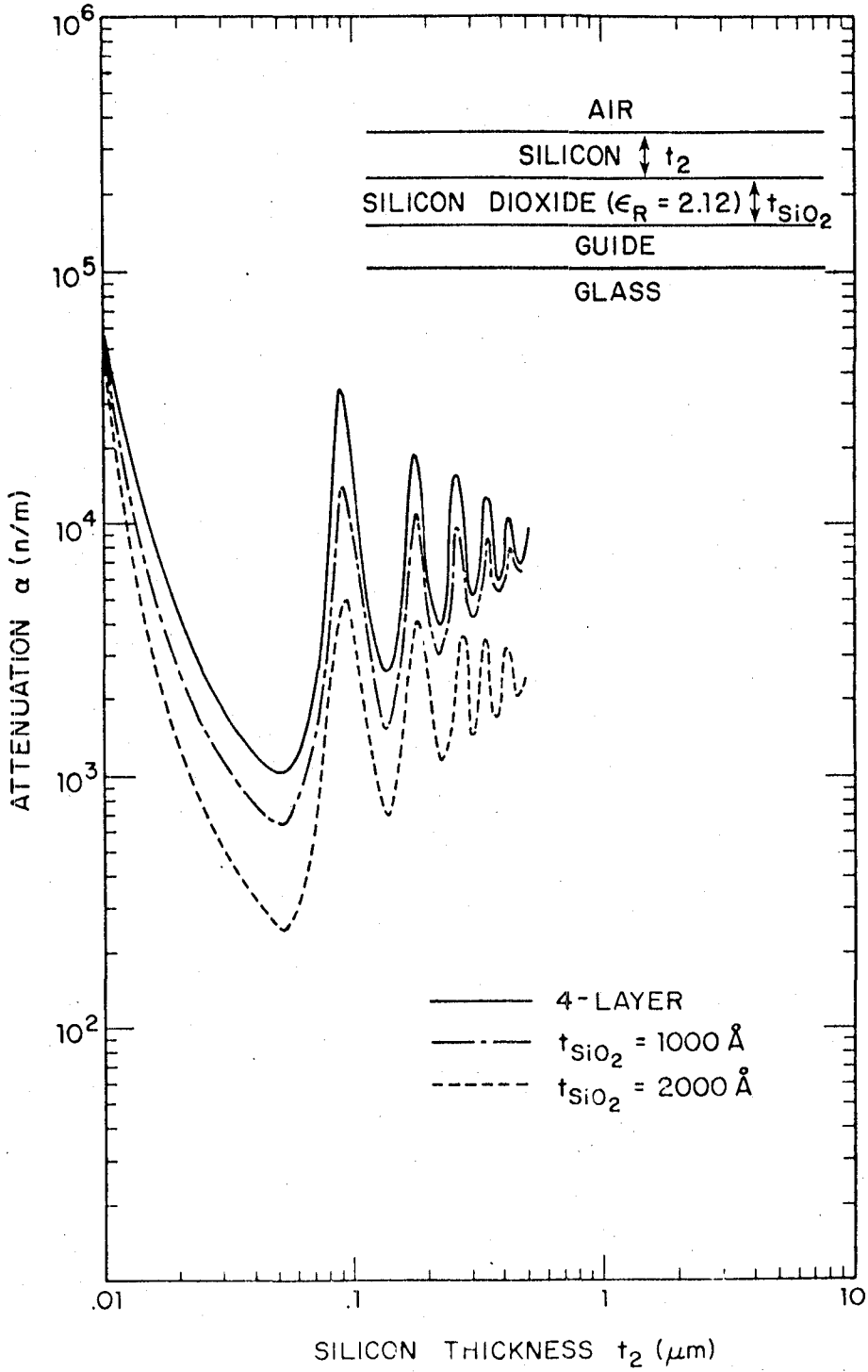

Figure 26. Attenuation Characteristics for 5-layer Structure

cont. case ii

Si Thickness (μm)		SiO_2 (ε_R = 2.12) thickness			
		100Å	500Å	1000Å	2000Å
.05	(local min)	-2.5%	-17%	-40%	-75%
.09	max	-5.8%	-30%	-56%	-84%
.13	min	-2.4%	-17%	-39%	-75%
.18	max	-1.5%	-14%	-37%	-74%
.22	min	-2.8%	-18%	-41%	-76%
.26	max	-2.6%	-18%	-42%	-76%

A significant decrease in attenuation is obtained by increasing the SiO_2 thickness.

Case iii

The attenuation constant (α) vs Si thickness is plotted for two different SiO_2 (ε_R = 2.387) thicknesses (1000, 2000Å) (Figure 27). The attenuation-Si thickness curve for the simple four-layer structure is shown for reference. The familiar damped sinusoidal behavior is apparent for both buffer layer thicknesses (1000, 2000Å), and the attenuation can be reduced significantly by a buffer layer. The percentage decrease in attenuation, relative to the four-layer values, for different buffer layer thicknesses is summarized below.

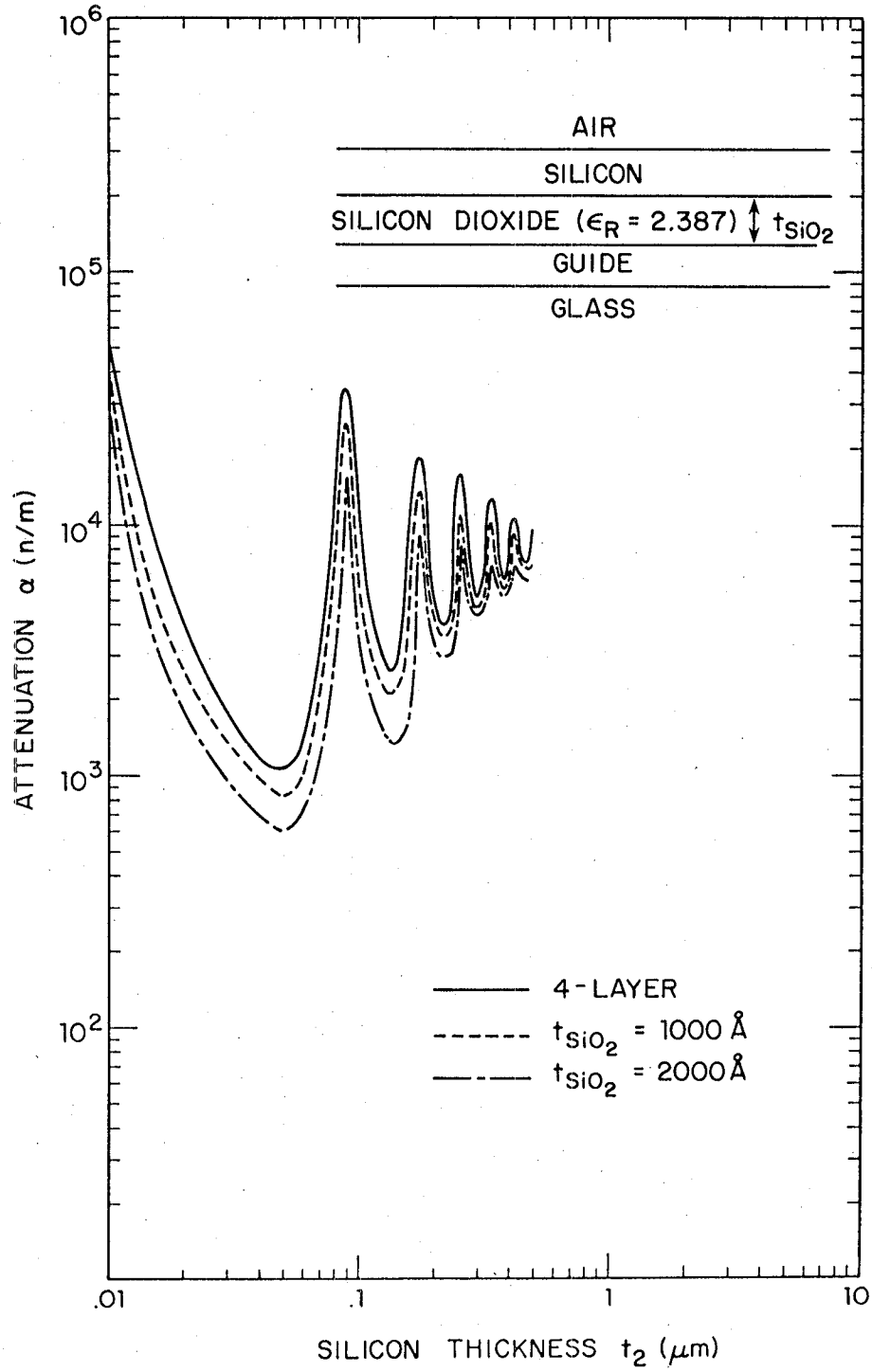

Figure 27. Attenuation Characteristics for 5-layer Structure

cont. case iii

Si Thickness (μm)		SiO_2 (ε_R = 2.387) thickness	
		1000Å	2000Å
.05	(local min)	-25%	-48%
.09	max	-30%	-54%
.13	min	-25%	-48%
.18	max	-23%	-47%
.22	min	-25%	-49%
.26	max	-25%	-49%

Again, a significant improvement is obtained by increasing the SiO_2 thickness.

Case iv

The attenuation constant (α) vs Si thickness is plotted for different SiO_2 (thickness = 1000Å) permittivities (ε_R = 2.12, 2.387) (Figure 28). The attenuation-Si thickness curve for the simple four-layer case is shown for reference. The familiar damped sinusiodal behavior is apparent for both cases, and the attenuation can be reduced significantly.

The percentage decrease in attenuation (relative to the four-layer values) for the different permittivities is summarized below.

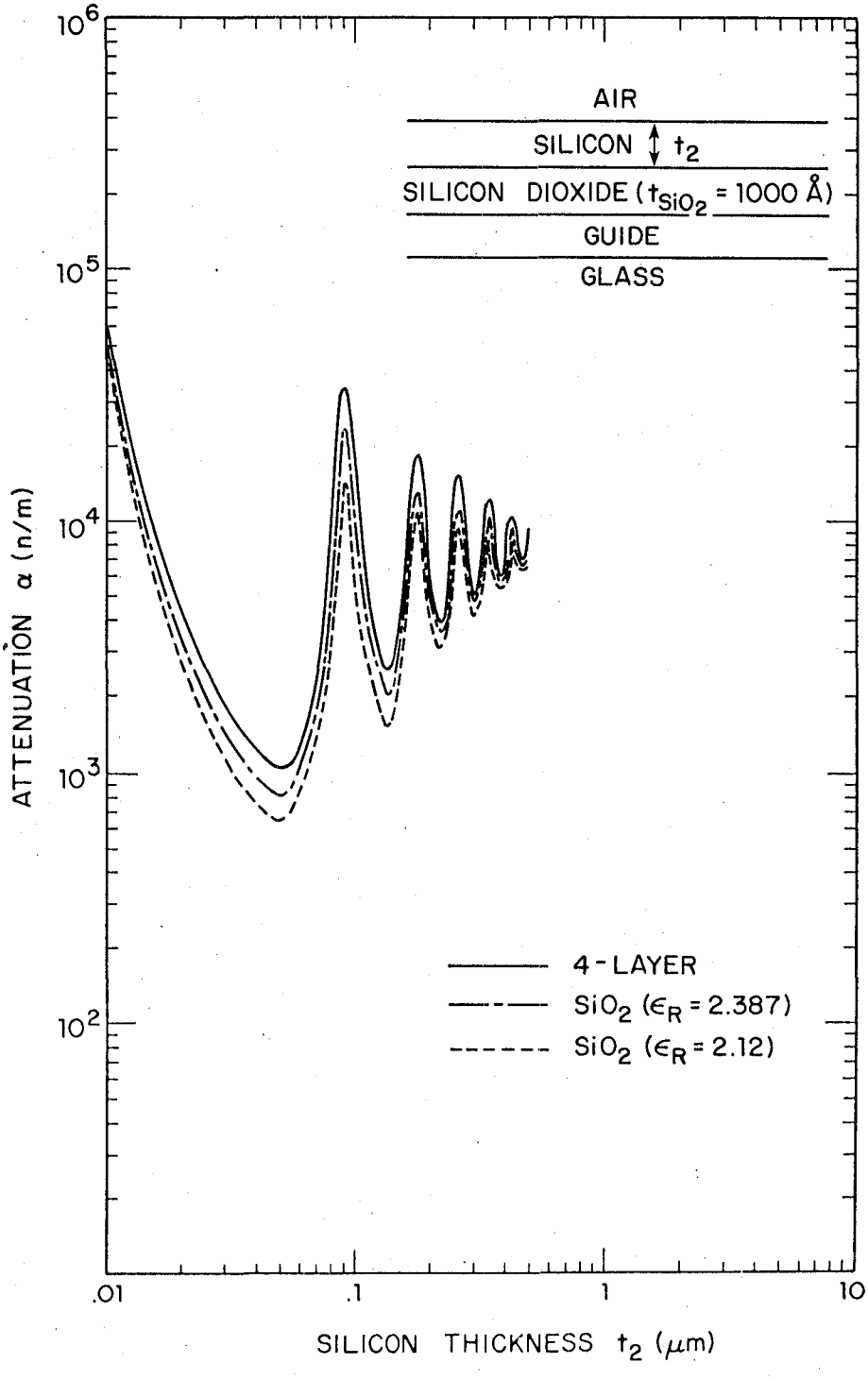

Figure 28. Attenuation Characteristics for 5-layer Structure

Si Thickness		SiO_2 (thickness = 1000Å) Permittivity	
		ε_R = 2.12	ε_R = 2.387
.05	(local min)	-40%	-25%
.09	max	-56%	-30%
.13	min	-39%	-25%
.18	max	-37%	-23%
.22	min	-41%	-25%
.26	max	-42%	-25%

SiO_2 (ε_R = 2.12) gives a more significant attenuation decrease.

Case v

The attenuation constant (α) vs Si thickness is plotted for different SiO_2 (thickness = 2000Å) permittivities (ε_R = 2.12, 2.387) (Figure 29). The attenuation vs Si thickness curve for the simple four-layer case is shown for reference. The familiar damped sinusoidal behavior is apparent for both buffer layers, and the attenuation can be reduced significantly.

The percentage decrease in attenuation (relative to the four-layer values) for the different permittivities is summarized below.

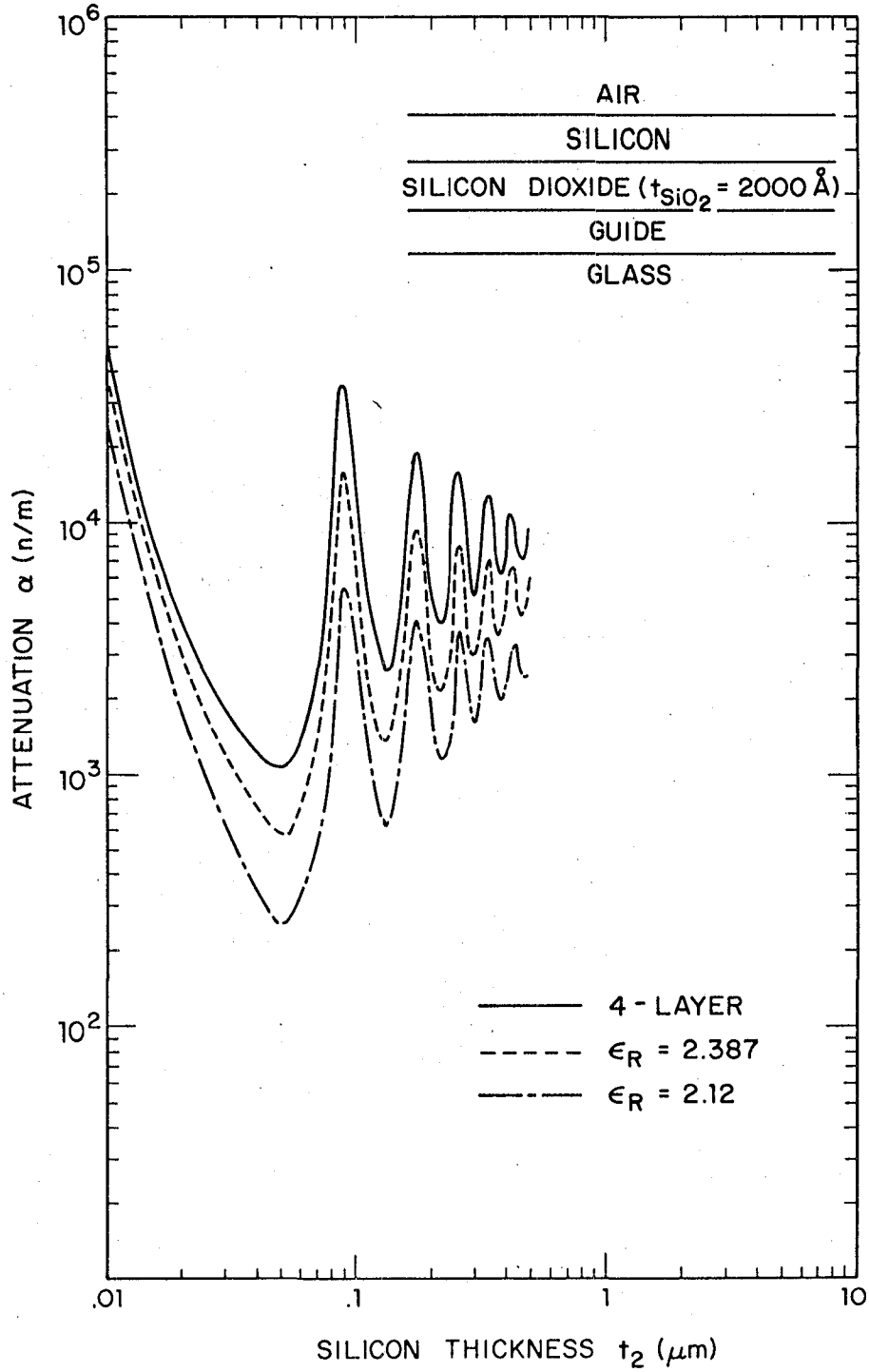

Figure 29. Attenuation Characteristics for 5-layer Structure

Si Thickness (μm)		SiO_2 (thickness = 2000Å) permittivity	
		$\varepsilon_R = 2.12$	$\varepsilon_R = 2.387$
.05	(local min)	-75%	-48%
.09	max	-84%	-54%
.13	min	-75%	-48%
.18	max	-74%	-47%
.22	min	-76%	-49%
.26	max	-76%	-49%

Again, SiO_2 ($\varepsilon_R = 2.12$) gives a more significant attenuation decrease.

These computer modeling studies indicate that the attenuation can be reduced significantly with the addition of an SiO_2 buffer layer between the guiding region and the semiconductor cladding. The familiar damped sinusoidal behavior is still evident for all five-layer cases considered; however, a slight decrease in the relative amplitude of the oscillations is apparent as the buffer layer thickness is increased which indicates a slight decrease in the attenuation shift for a given conductivity change. We also note that the attenuation can be more effectively reduced with a lower permittivity buffer layer. This is, at least, intuitively correct since the index of refraction of the buffer layer is less than that of the guide, and a lower index implies more confinement of the radiation to the guide. Conversely, computer studies indicate that the attenuation increases if the buffer layer has a higher index of refraction than the guide. Studies also indicate that a buffer layer increases β/K slightly, but decreases the amplitude of the

oscillations on the β/K-silicon thickness curve. For a practical device, then, an overall attenuation reduction with SiO_2 buffer layer must be carefully weighed against a decrease in the attenuation shift for a given conductivity change.

VI. SELENIUM-CLAD WAVEGUIDES

Several other semiconductors exhibit a damped sinusoidal behavior as the cladding layer thickness is increased. One substance, elemental selenium, appeared ideal for device applications.

Amorphous silicon, in contrast to the chalcogenide glasses (i.e. selenium), contains a large number of dangling bonds which form intergap states and fast recombination centers. The recombination sites limit the conductivity changes for all but the brightest intensities. One solution is to "passivate" with hydrogen which bonds to the silicon and effectively reduces the number of recombination centers (15).

Diffraction studies of selenium, however, indicate that the glass is comprised largely of helical chains and the evaporated or sputtered thin films have varying proportions of rings, as opposed to dangling bands; hence, passivation is not necessary. Furthermore, thin film deposition of selenium (melting temperature = 200^{o}C) can be easily accomplished by quenching from the melt (16, 17).

The preparation independent optical properties of selenium have been determined. At λ = .6328 μm, the complex permittivity $\hat{\varepsilon}$ = 7.9 + j1.0. Computer modeling of a selenium-clad dielectric waveguide again revealed the familiar damped sinusidal behavior of the attenuation vs thickness curve (Figure 30). Selenium, then, appeared ideal for device applications.

Unfortunately, further investigation revealed that thin film (<.3 μm) preparation from the melt is impossible and that this technique creates toxic selenium gas.

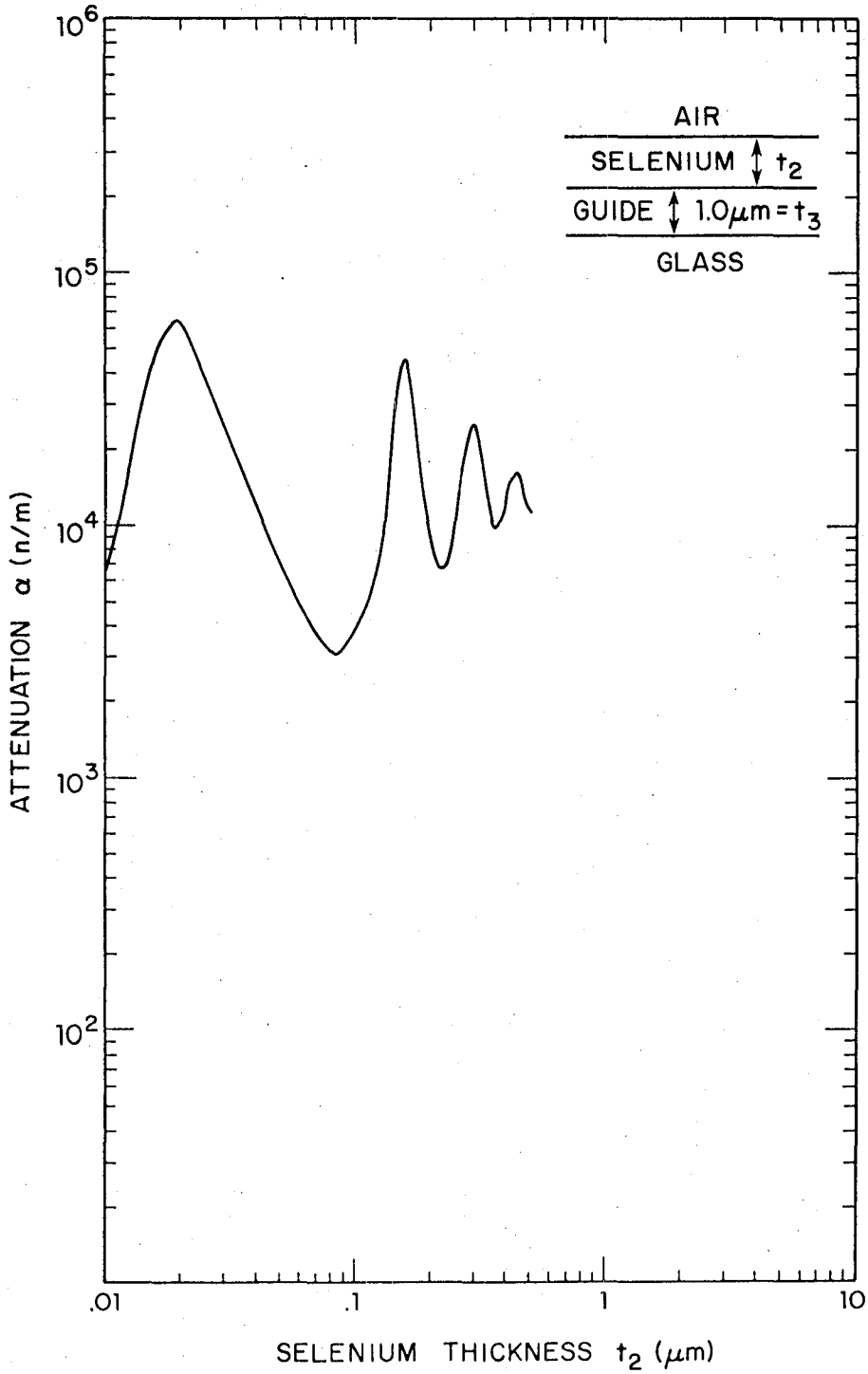

Figure 30. Attenuation Characteristics for Selenium-Clad Waveguide

VII. EXPERIMENTAL STUDIES

A. Ion-Exchange Waveguide Temperature Degradation

Several possible semiconductor deposition techniques were investigated including RF sputtering and vacuum deposition. Unfortunately, many methods involve subjecting the ion-exchange waveguides to high temperatures. Of particular interest, then, was the temperature degradation of the ion-exchange guides.

Fabrication procedures have been described in (18) and will only be briefly reviewed. The basic technique for ion-exchange optical waveguide fabrication is based upon the diffusion of silver ions into soda-lime glass and the replacement of sodium ions which diffuse out of the glass. The index of refraction (traditionally, a microscope slide) is raised, thereby forming a waveguide. The number of propagating modes is proportional to the diffusion time.

Several guides were prepared, and a table relating the number of propagating modes with the diffusion time is shown below.

Waveguide	Number of Modes	Diffusion Time
1 a and b	4/4	4 min
2 a and b	4/4	4 min
3 a and b	5/5	6 min
4 a and b	5/5	6 min
5 a and b	1/1	15 sec
6 a and b	1/1	15 sec
7 a and b	1/1	45 sec
8 a and b	1/1	45 sec
9 a and b	7/7	10 min
10 a and b	7/7	10 min

Some of these guides were heated to 300°C and then to 500°C, and the number of modes was observed.

Label	Modes (27°C)	Modes (300°C)	Modes (500°C)
Wave 1 a/b	4/4	4/4	DESTROYED
3 a/b	5/5	5/5	
5 a/b	1/1	1/1	
7 a/b	1/1	1/1	
9 a/b	7/7	7/7	

We note that all waveguides were able to support the same number of modes even after heating to 300°C; however, all guides were effectively "destroyed" after heating to 500°C. The conclusion, then, is that RF sputtering still is the ideal semiconductor deposition technique.

B. Design of Experimental Devices

Previous attempt to confirm the damp sinusoidal behavior of the four-layer silicon-clad optical waveguides have not been successful. Fortunately, an RF sputtering systems along with a silicon target was available for semiconductor deposition.

Radio frequency (RF) sputtering is a technique in which a source material (a target) is bombarded with gas ions accelerated by a high voltage. Particles from the target are ejected, traverse the vacuum chamber, and are subsequently deposited on a substrate as a thin film.

It was decided that a large number of waveguides would be sputtered with uniform silicon films ranging in thickness from .04μm to .40 μm in .01μm steps in order to confirm the damped sinusoidal behavior of the attenuation-silicon thickness curve. The uniform thickness silicon bar allows more accurate attenuation measurements because several measurements may be performed at different places on the guide and the results averaged. A 5 inch diameter silicon wafer was soldered to an aluminum holder and sputtering began.

A sputtering holder was designed and constructed which would allow the deposition of a silicon film 1μm wide and 20μm long on the waveguide surface.

In addition, a Hall probe mask was built in hopes that several sputtered silicon material characteristics (the material type, dopant concentration, and mobility) could be determined. Furthermore, Hall mask dimensions were designed so that a quick and accurate resistivity measurement could be made using a four-point probe (19).

Unfortunately, amorphous silicon (sputtered) is permeated with dangling bonds which render the sputtered silicon photoelectrically and photoconductively dead. This is less than ideal characteristics for an optical modulator which relies on photon-induced conductivity changes in the semiconductor cladding. These dangling bonds lie between the valence and conduction bands and act as fast, non-radiative recombination sites. One solution, however, is to sputter in hydrogen which effectively passivates the dangling bonds thereby revealing the interesting properties of silicon. Other atoms, including oxygen, nitrogen, and flourine may aid the passivation process.

The available system, however, only allows RF sputtering in argon and oxygen. Argon is completely ineffective for passivation, and oxygen is less than ideal. In fact, a number of sources expressed serious doubts about the possibility of passivation with oxygen. Fortunately, motivation was found in a number of obscure journal articles.

Paesler, Anderson et al (20) present the results of dark conductivity, photo-conductivity, photoluminescence, and optical absorption experiments on films of sputtered oxygenated amorphous silicon-hydrogen alloys. The authors conclude that oxygenated a - Si_{1-x} - H_x films exhibit photoconductive and photoluminescent response characteristic of glow-discharge films (i.e. passivation occurs).

Shimizu,Kumeda et al (21) prepared amorphous silicon with a low number of dangling bonds without the incorporation of hydrogen. The systems was pumped down to about 6×10^{-7} torr,

and 99.995% pure O_2 was introduced into the chamber to a pressure of approximately 1 x 10^{-5} torr. Argon was then introduced to a total pressure of 2 x 10^{-2} to 3 x 10^{-1} Torr.

Ishii, Naoe et al (22) significantly reduced the number of gap states in amouphous silicon by sputtering in an argon-oxygen mixture (O_2 partial pressure = 1 x 10^{-6} torr). Photoconductive properties comparable to those of hydrogenated amorphous silicon were observed.

The currently available vacuum system can realistically only pump down to a base pressure of 1 x 10^{-5} torr, which is not sufficient to duplicate the previous experiments; however, silicon was sputtered in an oxygen atmosphere (p = 1 x 10^{-3} torr) and a uniform layer of SiO_2 was obtained. Growth rate was approximately 1200Å/hr. A Dektac measurement along with a color calibration confirmed the film's uniformity. Many other films were sputtered in Ar-O_2 mixtures. Growth rates of approximately 1500Å/hr were obtained; however, tests indicated that the sputtered silicon was still photoelectrically dead so passivation was not realized. Finally, experiments were halted when the Si wafer continued to come unglued from the holder.

A new silicon sputtering target has been obtained and sputtering will begin again. Only confirmation of the damped sinusoidal behavior will be initially attempted (purely a bulk effect). Passivation, then, is not necessary, and argon will be used as the gas.

VIII. CONCLUSIONS

This study has led to several important conclusions about the development of direct modulation devices employing semiconductor clad optical waveguides. Based on this study and the following conclusions we believe such modulator are practical:

(1) Calculations using two different methods of solving the clad waveguide problem produce the same oscillatory behavior.

(2) The percent change in attenuation or phase shift is large.

(3) Similar experiments by other workers indicate the effect is real and useable in a device.

(4) Attenuation can be reduced significantly by inclusion of a buffer layer.

As pointed out in section 2 all calculations using both available computer programs verify the oscillating behavior of the attenuation and phase constant of the guided wave when clad by a thin silicon or GaAs films. The fact that the oscillations in phase and amplitude are 90^{o} out of phase allows the device to be designed as either a phase or amplitude modulator. The particular application originally invisioned for the direct optical modulator would require a phase modulator however the amplitude modulator might find application in communication circuits.

The percentage change in attenuation and phase with conductivity was large enough to make such a device feasible. The following table briefly summarizes these results for silicon films.

Film Thickness (μm)	% Change in	Changes in (%)	Phase Shift (rad/mm)
.14	50	42	<0.1
.14	25	22	<0.1
.17	50	<5	-4.8
.17	25	<3	-3
.22	50	35	<0.2
.22	25	19	<0.1

A main concern is whether a film <0.25 micrometers thick will absorb enough incident light to change the conductivity significantly. Previous calculations(23) have shown that the minimum predicted change in conductivity for a silicon film is 6.7% with a 50% change in light intensity. Even this produces a 0.6 radian/mm phase change and has provided encouragement to continue with experimental devices.

Lee and his co-workers (7) have constructed an optically con trolled millimeter-wave switch using conductivity changes in dielectric-clad waveguides and successfully demonstrated the modulation effect. Because of the lower frequency of the propagating wave, the silicon film was considerably thicker than that required for a direct optical modulator and thus a stronger

effect was observed than might be expected in thin films. From this data it appears that an optical device based on the same principal is worth building.

The buffer layer studies in section 5 indicte the potential reduction in attenuation possible through the use of a thin silicon dioxide film between the waveguide and the semiconductor. A 2000Å SiO_2 film reduces the attenuation by 75% so that a 1 mm long film (.13 mm thick, Si) would have an attenuation of about 2.1 dB which would be an acceptable loss for a phase modulator. In general the buffer layer allows us to shift the attenuation curve down while having no significant effect on the phase curve. This is an ideal control variable for either a phase or amplitude modulator.

Finally it should be mentioned that experimental data obtained from the one device fabricated was not conclusive and unfortunately technical problems with Si sputtering prevent fabrication of additional devices. Any future work must include experimental devices to verify the predicted oscillatory behavior. It is also evident that since the effect we are trying to make use of is predominate at film thickness of less than 1 micrometer the problem of absorption of the modulating signal must be addressed in greater detail. It may be necessary to couple the modulating signal into the thin semiconductor film through the use of a second guiding layer on top of the silicon film. These problems will be investigated in future work in this area.

References

1. C. M. Verber, D. W. Vekey, V. E. Wood, R. P. Kenan and N. F. Hartman, "Feasibility Investigaion of Integrated Optics Fourier Transform Devices", NASA Contractor Report, July 1977, NASA CR 2869.

2. T. E. Batchman, "Investigation of Direct Integrated Optics Modulators", Semi-Annual Status Report, NASA Grant NSG 1567, UVA Report No. 52 8171/EE79/01, July 1979.

3. T. E. Batchman, "Investigation of Direct Integrated Optics Modulators", Semi-Annual Status Report, NASA Grant NSG 1567, UVA Report No. 52 8171/EE80/104, October 1980.

4. I. P. Kaminow, W. L. Mammel, and H. P. Weber, "Metal-Clad Optical Waveguides: Analytical and Experimental Study", Appl. Opt., Vol. 13, pp. 296-405, February 1974.

5. J. W. Bandler and P. A. Macdonald, "Optimization of Microwave Networks by Razor Search", IEEE Trans. on Microwave Theory and Techniques, Vol. MTT-17, No. 8, 1969, pp. 552-652.

6. R. B. Smith and G. L. Mitchell, "Calculation of Complex Propagating Modes in Arbitrary, Plane-Layed, Complex Dielectric Structures", EE Technical Report No. 206, University of Washington, NSF Grant ENG 76-09937.

7. C. H. Lee, P. S. Mak, and A. P. DeFonzo, "Optical Control of Millimeter-Wave Propagation in Dielectric Waveguides", IEEE Trans. on Quantum Electronics, Vol. QE-16, No. 3, March 1980, pp. 277-288.

8. O. S. Heavens, Optical Properties of Thin Solid Films, Academic Press, Inc. New York, 1955, pp. 1970-172.

9. J. D. Stratton, Electromagnetic Theory, McGraw-Hill Book Co., New York,1941, pp. 515-516.

10. V. A. Kiselev, "Diffraction Coupling ofRadiation into a Thin-film Waveguide," Sov. J. of Quantum Electron, Vol. 4, pp. 872-875, January 1975.

11. A. A. Zlenko, V. A. Kiseleve, A. M. Prolchoror, A. A. Spikhalskii, and V. A. Sychugov, "Emission of Surface Light Waves from A corrugated Part of a Thin-film Guide," Sov. J. of Quantum Electron, Vol 4, pp. 839-842, January 1975.

12. K. C. Chang and T. Tamir, "Bragg-Reflection Approach for Blazed Dielectric Grating," Optics Communications, Vol. 26, Number 3, pp. 327-330, September, 1978.

13. K. C. Chang, V. Shah, and T. Tamir, "Scattering and Guiding of Waves by Dielectric Gratings with Arbitrary Profiles," J. Opt. Soc. Amer., Vol. 70, Number 7, pp. 804-813, July 1980.

14. S. C. Rashleigh, Planar Metal-Clad Dielectric Optical Waveguides, Ph.D. Thesis, University of Queensland, Brisbane Australia, May 1975, pp. 190-213.

15. M. H. Brodsky, ed. "Amorphous Semiconductors," Topics in Applied Phyics, Vol. 36, (New York), Springer Verlag, 1979, pp. 1-7.

16. T. Fischer, "Luminescence in Amorphous Semiconductors," Topics in Applied Physics, Vol. 36, (New York), Springer Verlag, 1979, pp. 176-180.

17. D. E. Harrison, "The Viscosity of Liquid Selenium," Recent Advances in Selenium Physics, Pergamon Press, London, 1965, pp. 67-85.

18. K. Gates and T. E. Batchman, "Fabrication of Ion Exchanged Optical Waveguides," Southeastcon '80 Proceedings, April 13, 1980.

19. L. B. Valdes, "Resistivity Measurements on Germanium for Transistors," Proceedings of the IRE, Vol. 42, Number 420, pp. 420-427, February 1954.

20. M. Paesler and D. Anderson, "New Developments in the Study of Amorphous Silicon Hydrogen Alloys," Physical Review Letters, Vol. 41, Number 21, pp. 1492-7, November 20, 1978.

21. T. Shimizu and M. Kumeck, "Influence of Oxygen and Depositon Conditions of RF-Sputtered Amorphous Si Film," Jpn. J. Appl. Phys., Vol. 18, Number 10, pp. 1923-9, October 1979.

22. K. Ishii and M. Naoe, "Electrical Properties of Oxygenated Amorphous Si Prepared by Ion-Beam Sputters," Jpn. J. Appl. Phys., Col. 18, No. 7, pp. 1395-6, 1979.

23. T. E. Batchman, "Investigation of Direct Integrated Optics Modulators," Annual State Report, NASA Grant NSG 1567, UVA Report No. 528171/EE80/102, March 1980.

DISTRIBUTION LIST

Copy No.	
1 - 2	NASA Scientific and Technical Information Facility P. O. Box 8757 Baltimore/Washington International Airport Baltimore, MD 21240
3 - 5	FED - Electron Device Research M/S 473 NASA Langley Research Center Hampton, VA 23665 ATTN: M. E. Beatty, III
6 - 12	T. E. Batchman
13	E. A. Parrish, Jr.
14	I. A. Fischer Office of Sponsored Programs
15 - 16	E. H. Pancake Clark Hall
17	RLES

End of Document